

University of New Hampshire
University of New Hampshire Scholars' Repository

Master's Theses and Capstones

Student Scholarship

Fall 2009

Computational studies on complex reaction mechanics

Alicia C. Voukides

University of New Hampshire, Durham

Follow this and additional works at: <https://scholars.unh.edu/thesis>

Recommended Citation

Voukides, Alicia C., "Computational studies on complex reaction mechanics" (2009). *Master's Theses and Capstones*. 500.
<https://scholars.unh.edu/thesis/500>

This Thesis is brought to you for free and open access by the Student Scholarship at University of New Hampshire Scholars' Repository. It has been accepted for inclusion in Master's Theses and Capstones by an authorized administrator of University of New Hampshire Scholars' Repository. For more information, please contact nicole.hentz@unh.edu.

COMPUTATIONAL STUDIES ON COMPLEX REACTION MECHANISMS

BY

Alicia C. Voukides

B.S., Bates College, 2007

THESIS

Submitted to the University of New Hampshire
in Partial Fulfillment of
the Requirements for the Degree of

Master of Science

in

Chemistry

September, 2009

UMI Number: 1472087

INFORMATION TO USERS

The quality of this reproduction is dependent upon the quality of the copy submitted. Broken or indistinct print, colored or poor quality illustrations and photographs, print bleed-through, substandard margins, and improper alignment can adversely affect reproduction.

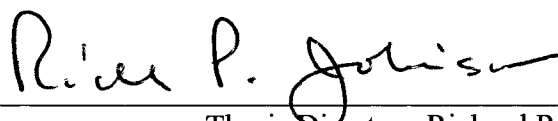
In the unlikely event that the author did not send a complete manuscript and there are missing pages, these will be noted. Also, if unauthorized copyright material had to be removed, a note will indicate the deletion.

UMI[®]

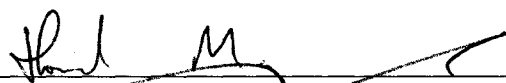
UMI Microform 1472087
Copyright 2009 by ProQuest LLC
All rights reserved. This microform edition is protected against
unauthorized copying under Title 17, United States Code.

ProQuest LLC
789 East Eisenhower Parkway
P.O. Box 1346
Ann Arbor, MI 48106-1346

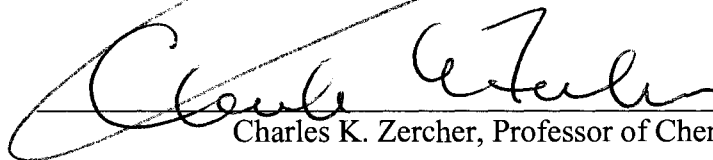
This thesis has been examined and approved.



Thesis Director, Richard P. Johnson
Professor of Chemistry



Howard R. Mayne, Professor of Chemistry



Charles K. Zercher, Professor of Chemistry

August 13, 2009

Date

ACKNOWLEDGEMENTS

First and foremost, I must sincerely thank the Department of Chemistry for taking a chance on me as a math major.

To:

Dr. Johnson for his patience and guidance.

The graduate school for the summer fellowship that allowed me to finish this summer.

Dr. and Mrs. Alvin R. Ingram for the award for which I am grateful and honored.

Jesse Farnham for a UNIX script that runs Gaussian.

My parents, Charles and Carol, and my brother, Chris: a family worth being proud of.

And of course, Steve for being Steve.

TABLE OF CONTENTS

ACKNOWLEDGEMENTS.....	iii
LIST OF SCHEMES.....	vi
LIST OF FIGURES	ix
LIST OF TABLES.....	xi
ABSTRACT.....	xii
CHAPTER	PAGE
I. REACTIONS OF OZONE WITH CARBONYL COMPOUNDS AND BIMOLECULAR OZONE DECOMPOSITION.....	1
Introduction	1
Ozone + Aldehydes	1
Ozone + Ketones	3
Aqueous Ozone Decomposition	4
Results and Discussion	7
Formaldehyde + Ozone	7
Acetone + Ozone	11
Bimolecular Ozone Decomposition	13
Conclusions	16
II. THE DOERING-MOORE-SKATTEBØL REARRANGEMENT.....	18
Introduction	18

Results and Discussion	21
Chiral Carbenoids.....	25
<i>Trans</i> C9	30
<i>Cis</i> C9	32
Dimers	37
Conclusions	44
III. BIS-LACTAM CYCLIZATIONS	47
Introduction	47
Results and Discussion	50
Conclusions	53
IV. THERMAL REARRANGEMENTS OF ORTHO-ETHYNYLTOLUENE	54
Introduction	54
Results and Discussion	56
Conclusions	63
LIST OF REFERENCES.....	64
APPENDIX.....	74
COMPUTATIONAL DETAILS	75

LIST OF SCHEMES

NUMBER	PAGE
1-1	Reaction of octanal and ozone as drawn in 1910 depicting the formation of a tetroxolane.....1
1-2	The concerted nucleophilic addition of ozone to benzaldehyde proposed by White and Bailey.....2
1-3	Isobutyraldehyde undergoes label exchange in the presence of ozone, as shown by Klopman and Joiner.....2
1-4	The two likely reaction pathways in the ozonation of formaldehyde7
1-5	UM05-2X/6-311+G(d,p) [UCCSD(T)//UM05-2X] energetics for the two pathways in the oxidation of formaldehyde by ozone.....8
1-6	UM05-2X/6-311+G(d,p) [UCCSD(T)//UM05-2X] energetics for the oxidation of acetone by ozone11
2-1	The Doering-Moore-Skattebøl Rearrangement18
2-2	Concerted and stepwise pathways from lithium-bromine carbenoid 12R to allene 13R proposed by Azizoglu, et al.20
2-3	CCSD(T)//B3LYP/6-311+G(d,p) energetics and geometries for the two pathways of the Doering-Moore-Skattebøl Rearrangement.....22
2-4	B3LYP/6-311+G(d,p) energetics for the formation of <i>S</i> -2,3-pentadiene (17) from <i>trans</i> -1-bromo-2,3-dimethyl-1-lithiocyclopropane (15).....26
2-5	B3LYP/6-311+G(d,p) energetics for parent carbenoid (12-OMe₂) explicitly solvated by complexation with two dimethyl ether molecules28
2-6	Implicit solvation for the ring opening of parent carbenoid (12-PCM) computed at B3LYP/6-311+G(d,p) with PCM solvation in diethyl ether.....31
2-7	B3LYP/6-31+G(d) energetics for the ring opening of <i>trans</i> bicyclic carbenoid 18 to (<i>R</i>)-1,2-cyclononadiene (20)31
2-8	B3LYP/6-31+G(d) energetics showing lithium-halogen exchange with the diastereotopic bromines in 21 to form two <i>cis</i> bicyclic carbenoids 23 and 2433

2-9	B3LYP/6-31+G(d) energetics for ring opening of the two <i>cis</i> bicyclic carbenoids 23 and 24	34
2-10	Implicit solvation for the ring opening of the two <i>cis</i> carbenoids 23-PCM and 24-PCM computed at B3LYP/6-31+G(d) with PCM solvation in diethyl ether.....	36
2-11	Implicit solvation for the ring opening of <i>trans</i> bicyclic carbenoid 18-PCM computed at B3LYP/6-31+G(d) with PCM solvation in diethyl ether	37
2-12	B3LYP/6-31+G(d) and B3LYP/6-31+G(d) with PCM solvation in diethyl ether energies and free energies in kcal/mol for dimerization of bent carbenoid 12	38
2-13	B3LYP/6-31+G(d) and B3LYP/6-311+G(d,p) energetics for the ring opening of parent dimer 12D	39
2-14	Implicit solvation for the ring opening of the parent dimer 12D-PCM computed at B3LYP/6-31+G(d) with PCM solvation in diethyl ether	40
2-15	B3LYP/6-311+G(d,p) energetics and geometries for dimerization of bent dimethyl carbenoid 28	41
2-16	B3LYP/6-31+G(d) and B3LYP/6-311+G(d,p) energetics for the ring opening of dimethyl dimer 29	41
3-1	Proposed conjugate addition mechanism for the cyclization of bis-lactam 40-H	48
3-2	M05-2X/6-31G(d) energetics of the first anionic cyclization of bis-lactam 40-H	51
3-3	M05-2X/6-31G(d) energetics of the second anionic cyclization of bis-lactam 40-H	52
3-4	M05-2X/6-31G(d) energetics for the neutral minima in the cyclization of bis-lactam 40-H	52
3-5	Concerted [4+4] cycloaddition mechanism for the cyclization of bis-lactam 40-H	53
4-1	The Brown Rearrangement	54
4-2	Isotopic scrambling seen by Brown in 1974, suggesting phenylacetylene is in equilibrium with benzyliidenecarbene.....	54

4-3	Summary of the products from the pyrolysis of o-ethynyltoluene	55
4-4	Summary of the competitive processes in the thermal rearrangement of o-ethynyltoluene to yield indene and chrysene	55
4-5	B3LYP/6-311+G(d,p) energies and free energies at 898 K for the thermal rearrangement of o-ethynyltoluene to indene and the reactive intermediate ortho-xylallene	57
4-6	CCSD(T)/6-311G(d)//B3LYP/6-311+G(d,p) energetics for the thermal rearrangement of o-ethynyl toluene	57
4-7	Dimerization of ortho-xylallene	59
4-8	Comparisons of the B3LYP/6-311+G(d,p) energies for the [1,5] versus the C-H insertion transition states for the structural variations of ene-yne 62	61
4-9	Potential application of the chemistry of o-xylallene calculated at B3LYP/6-311+G(d,p)	62

LIST OF FIGURES

NUMBER		PAGE
1-1	UCCSD(T)//UM05-2X/6-311+g(d,p) energetics and UM05-2X/6-311+g(d,p) geometries for the abstraction pathway in the ozonation of formaldehyde	9
1-2	UCCSD(T)//UM05-2X/6-311+g(d,p) energetics and UM05-2X/6-311+g(d,p) geometries for the addition pathway in the ozonation of formaldehyde	10
1-3	UCCSD(T)//UM05-2X/6-311+g(d,p) energetics and UM05-2X/6-311+g(d,p) geometries for the addition pathway in the ozonation of acetone	12
1-4	UCCSD(T)//UM05-2X/6-311+g(d,p) energetics and UM05-2X/6-311+g(d,p) geometries for the abstraction pathway in the ozonation of acetone	13
1-5	UCCSD(T)//UB3LYP/6-311+G(d,p) energetics and UB3LYP/6-311+G(d,p) geometries for the bimolecular decomposition of ozone	14
1-6	Spin density at UB3LYP/6-311+G(d,p) showing two triplet oxygens of opposite spin, one red and the other blue, and one singlet oxygen resulting from the bimolecular decomposition of ozone	14
2-1	Historical milestones in the Doering-Moore-Skattebøl Rearrangement	19
2-2	Triangular and linear geometries for lithium-bromine carbenoids	19
2-3	CCSD(T)//B3LYP/6-311+G(d,p) energies and geometries for the two carbenoid minima	21
2-4	Natural charge densities at B3LYP/6-311+G(d,p) for the bent and linear carbenoids.....	23
2-5	B3LYP/6-311+G(d,p) intrinsic reaction coordinate showing initially disrotatory ring opening followed by conrotatory ring opening in the Doering-Moore-Skattebøl Rearrangement	24

2-6	Sample topology of a valley ridge inflection point where the surface curvature changes. The test function depicted is $f(x,y) = yx^2 + 0.2y^2$	25
2-7	B3LYP/6-311+G(d,p) intrinsic reaction coordinate showing the disrotatory ring opening of <i>trans</i> dimethyl carbenoid 15 to yield <i>S</i> -2,3-pentadiene (17)	27
2-8	Dissociation energies and free energies at -30° C for the starting carbenoid (12), transition state (TS16), and allene (13) in the Doering-Moore-Skattebøl Rearrangement computed at B3LYP/6-311+G(d,p) with PCM solvation in diethyl ether.....	30
2-9	B3LYP/6-31+G(d) forward intrinsic reaction coordinate showing the disrotatory ring opening of <i>trans</i> bicyclic carbenoid 18 through TS23A to (<i>R</i>)-1,2-cyclononadiene (20)	32
2-10	B3LYP/6-31+G(d) intrinsic reaction coordinate showing the disrotatory ring opening of carbenoid 24 through TS30A to 1,2-cyclononadiene (20).....	35
2-11	B3LYP/6-31+G(d) forward intrinsic reaction coordinate for ring opening of dimethyl dimer 29 through TS34	42
2-12	B3LYP/6-31+G(d) forward intrinsic reaction coordinate for ring opening of dimethyl dimer 29 through TS35	43
3-1	Summary and M05-2X/6-31G(d) geometries of the major products from the cyclization of bis-lactam 40-H	49
4-1	CCSD(T)/6-311G(d)//B3LYP/6-311+G(d,p) energetics and B3LYP/6-311+G(d,p) geometries for the thermal rearrangement of <i>o</i> -ethynyltoluene (50) to <i>o</i> -xylallene (54) and indene (51)	58
4-2	B3LYP/6-311+G(d,p) energetics and geometries for the dimerization of <i>ortho</i> -xylallene	59

LIST OF TABLES

NUMBER		PAGE
1	Comparison of calculated activation energies and exothermicities at different levels of theory for the bimolecular decomposition of ozone.....	15
2	Reaction energetics for the Doering-Moore-Skattebøl Rearrangement compared over several computational methods	22
3	¹³ C chemical shifts of the carbenoid carbon relative to TMS calculated at B3LYP/6-311+G(2d,p)	44

ABSTRACT

COMPUTATIONAL STUDIES ON COMPLEX REACTION MECHANISMS

by

Alicia C. Voukides

University of New Hampshire, September, 2009

Molecular modeling with density functional and higher level methods was used to study mechanisms for the reactions of carbonyl compounds with ozone, the Doering-Moore-Skattebøl Rearrangement, bis-lactam cyclizations, and thermal rearrangements of ortho-ethynyltoluene. Ozonation of both formaldehyde and acetone can proceed by one of two slow pathways: stepwise addition across the carbonyl group or hydrogen atom abstraction. The Doering-Moore-Skattebøl Rearrangement proceeds as a triangular lithium-halogen carbenoid, opening stereospecifically to an allene, with lithium-halogen dissociation occurring after the transition state. Bis-lactam cyclization is rapid, reversible, and thermodynamically controlled. The experimentally observed major product is confirmed by computations as thermodynamically most stable. Thermal rearrangements of o-ethynyltoluene proceed through competitive [1,2] and [1,5] H-shifts. Chrysene is formed as a minor product by dimerization of a novel intermediate, ortho-xylallene.

CHAPTER I

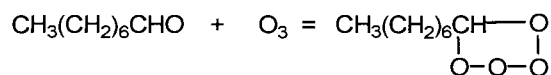
REACTIONS OF OZONE WITH CARBONYL COMPOUNDS AND BIMOLECULAR OZONE DECOMPOSITION

Introduction

Ozone + Aldehydes. Although the reaction of aldehydes with ozone has been studied for more than 100 years, it has remained poorly understood. Assorted theoretical and experimental studies have come to seemingly contradictory conclusions, indicative of a multifaceted scheme rather than a single pathway.

Harries and Langheld published the first study of an aldehyde-ozone reaction in 1903, suggesting that the reaction of octanal and ozone proceeds through a 5-membered ring, now called a tetroxolane.¹⁻³

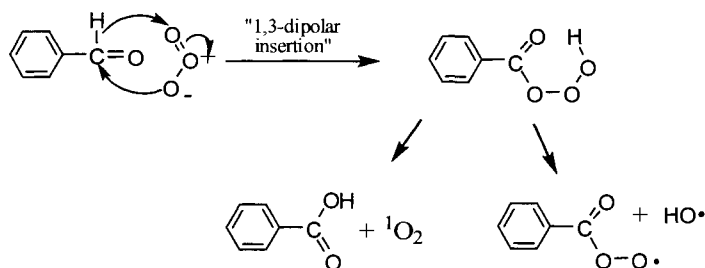
Scheme 1-1. Reaction of octanal and ozone as drawn in 1910 depicting the formation of a tetroxolane.³



Since this first report, many experiments and theoretical studies offered evidence not only for tetroxolanes, but also peracids and hydrotrioxides as intermediates.⁴⁻²² Briner, for example, ozonized benzaldehyde in the 1930s, focusing on ozone as a catalyst, and isolated both benzoic and perbenzoic acid.^{4, 6-10} In 1964, Dick and Hanna also recovered perbenzoic acid in high yield in the ozonation of benzaldehyde.¹⁵ In perhaps the most significant early study, White and Bailey proposed in 1965 what they termed a “1,3-dipolar insertion” for the reaction of benzaldehyde with ozone, a concerted mechanism

whereby ozone inserts into the C-H bond.¹⁷ This process leads directly to a hydrotrioxide, which they suggest can decompose in several ways to an assortment of species, including benzoic acid and singlet oxygen.

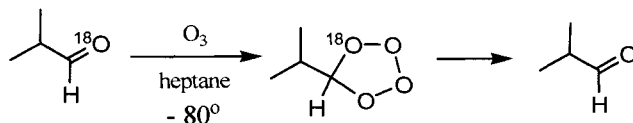
Scheme 1-2. The concerted nucleophilic addition of ozone to benzaldehyde proposed by White and Bailey.¹⁷



White and Bailey's 1,3-dipolar insertion remained the accepted mechanism for the reaction of ozone with aldehydes, as many groups continued to find corroborating evidence. Soon after its publication, Erickson et al. observed deuterium isotope effects consistent with White and Bailey's ionic mechanism.¹⁸ They also considered the possibility of a 5-membered tetroxolane, but suggested that it was a minor intermediate that rearranged to the same hydrotrioxide. In 1974, Murray and coworkers observed the $-OOH$ resonance of this same hydrotrioxide at 13.1 ppm by ¹H NMR.^{20, 21}

Further evidence for a tetroxolane intermediate was reported in 1975 when Klopman and Joiner reported that ¹⁸O-labeled isobutyraldehyde undergoes a label exchange when treated with ozone at -80 °C.^{23, 24} They proposed the reversible formation of a tetroxolane by a 1,3-dipolar addition of ozone across the carbonyl, followed by a cycloreversion. They did not consider any oxidation processes.

Scheme 1-3. Isobutyraldehyde undergoes label exchange in the presence of ozone, as shown by Klopman and Joiner.^{23, 24}



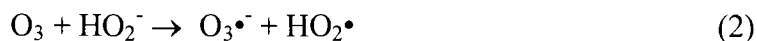
As White and Bailey had proposed, aldehyde-ozone reactions were commonly accepted as ionic mechanisms, with radical species produced in successive fragmentation steps. In a review in 1982, Martinez supported a cycloaddition mechanism across the carbonyl double bond, analogous to alkene ozonolysis.²⁵ In 1986, Pryor and coworkers ozonized pivaldehyde to obtain a hydrotrioxide, reporting an activation energy of 8.6 kcal/mol.²⁶ The field remained nearly dormant until 2007, when Yang and coworkers studied reactions of acetaldehyde with ozone by computation.²⁷ They considered both acyl and alpha hydrogen atom abstraction using DFT and higher level methods. These authors predicted that acyl hydrogen atom abstraction of acetaldehyde is endothermic by 13.0 kcal/mol and has an activation energy of 18.8 kcal/mol, but alpha hydrogen atom abstraction is endothermic by 18.2 kcal/mol with a barrier of 35.4 kcal/mol. In 2009, Plesnicar et al. also studied the ozonation of benzaldehyde experimentally and by computation.²⁸ They supported White and Bailey's 1,3-dipolar addition mechanism, but their conclusion is erroneous since the wavefunction for this concerted process is unstable relative to becoming open shell. They declared the hydrotrioxide, not the tetroxolane, as the key intermediate, but claimed that it decomposed too quickly for detection by NMR.

Ozone + Ketones. Reactions of ozone with ketones have not been as extensively studied as those with aldehydes. Most are kinetic rather than mechanistic studies and focus on the enol rather than the ketone. The only known experimental evidence of a reaction with ozone and a ketone is the M.S. thesis research of Kaleen M. Konrad (2006).²⁹ DFT and CBS-QB3 calculations predicted a stepwise mechanism with a modest barrier for the reaction of ozone with acetone. Experimental studies with several ¹⁸O-labeled ketones,

including 4-*t*-butyl-cyclohexanone, acetophenone, and benzophenone showed label exchange when treated with ozone. The tetroxolane was emphasized as the intermediate responsible for the loss of the ^{18}O label, just as Klopman concluded in 1975.^{23,24}

Aqueous Ozone Decomposition. The chemistry of ozone in water is complex and highly dependent on pH. As a powerful oxidant, ozone is widely used for water purification. Aqueous ozone chemistry is often attributed to the hydroxy radical, as proposed by Hoigné,^{30,31} but there remains some uncertainty about how this species may be produced in solution. The ability of ozone to purify water must depend on its concentration, which, in turn, is affected by ozone decomposition. It has long been known that solutions of ozone decompose, likely to oxygen and hydrogen peroxide, but this mechanism has been poorly understood. Studies on aqueous ozone emphasize pH dependence and most concur that decomposition is a chain process initiated by hydroxide ions, though the order of the reaction has been widely disputed. Many groups also assert that the reaction order varies with pH. A litany of radical and ion intermediates have been proposed, including $\text{HO}\cdot$,³⁰⁻³³ $\text{HOO}\cdot$,³²⁻³⁴ HOO^{-34} , $\text{HOOO}\cdot$,^{33, 35} HO_4^{-} ,³⁵ HO_5^{-} ,³⁵ H_2O_4 ,^{36, 37} $\text{O}_2\cdot^{-}$,³⁸ and $\text{O}_3\cdot^{-}$.³⁸ Several reviews of aqueous ozone chemistry attempt to sort through the various proposed models.³⁸⁻⁴⁴

Rothmund and Burgstaller studied the kinetics of aqueous ozone decomposition in 1913, and were first to conclude that decomposition is slow in acidic solutions and rapid in basic solutions.⁴⁵ In 1935, Weiss proposed the now widely accepted two-step chain initiation³⁴



Stumm provided the first kinetic model of ozone decomposition in water in 1954, stressing its dependence on hydroxide.⁴⁶ For a pH range of 7.6-10.4, he reported decomposition is first order in ozone and 0.75 order in hydroxide. Kilpatrick and coworkers (1956) reported that decomposition is 3/2 order in O₃ at low pH, but deviates significantly at high pH.⁴⁷ In 1971, Hewes and Davidson reported a second order reaction at low pH, which becomes first order at pH 8.⁴⁸ They also suggest the rate of decomposition becomes increasingly pH-sensitive as the solution is made more alkaline, further evidence of hydroxide dependence. Gurol and Singer (1982) found ozone decomposition to be second order in ozone and 1/2 order in hydroxide above pH 4.⁴⁹ Gordon et al. proposed a mixed rate law, with a first and a second order term for ozone, suggesting that at high pH and in the presence of radical scavengers, the second order term disappears.⁵⁰ They later supported this assertion by numerical simulations.⁵¹

$$r_{\text{O}_3} = k_1[\text{O}_3][\text{OH}^-] + k_2[\text{O}_3]^2[\text{OH}^-] \quad (3)$$

Sotelo et al. (1987) suggest a slightly different mixed rate law, which is valid in both acidic and basic solutions⁵²

$$r_{\text{O}_3} = k_A[\text{O}_3] + k_B[\text{OH}^-]^{1/2}[\text{O}_3]^{3/2} \quad (4)$$

In 2001, von Sonntag et al. found nearly 100% yield of singlet oxygen in many aqueous ozone reactions, suggesting that it forms by O-atom transfer.³⁷ In 2005, Kuosa, Haario, and Kallas obtained a reaction order of 1.12 with respect to ozone and 0.51 with respect to hydroxide.⁵³ In a 2006 review, Fábíán discussed several reactive intermediates in

aqueous ozone decomposition, stressing HO• as the chain carrier at low pH and the ozonide anion O₃^{•-} at higher pH.³⁸

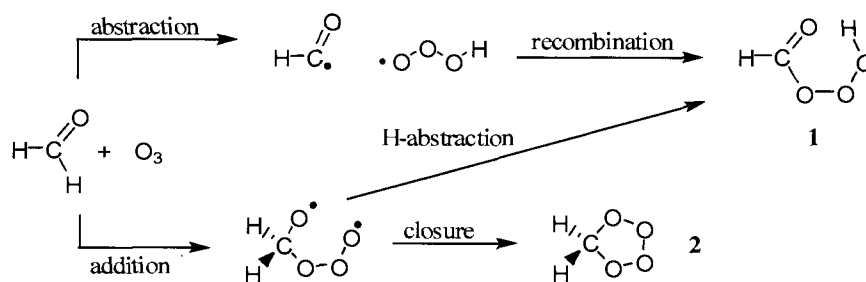
One of the clearest experimental studies was reported only recently. In 2008, Ershov and Morozov showed that aqueous ozone decomposes at pH 4-8 by a bimolecular reaction according to the equation $O_3 + O_3 \rightarrow 3O_2$ with a rate order of 1.9 ± 0.2 and an activation energy of 18.2 ± 2 kcal/mol.⁵⁴ They also maintain that decomposition is catalyzed by hydroxide ions. Most recently, Lovato and coworkers compiled a “well accepted 18-step mechanism” for the decomposition of ozone in water.⁵⁵ This “mechanism” is not intended to represent the sequential steps of ozone decomposition, but rather summarize the major processes of aqueous ozone chemistry. As with the previous reports, they suggest that decomposition is initiated by the reaction of ozone with hydroxide anion to give a hydroperoxy anion and molecular oxygen. The seventeen steps that follow encompass the many steps proposed in earlier kinetic models. This series of proton, electron, and oxygen transfers ultimately results in the production of hydrogen peroxide and molecular oxygen.

While each of these steps may be occurring in solution, the complexity of the mechanism seems to contradict Ershov and Morozov’s recent results,⁵⁴ which suggest a bimolecular reaction with a modest barrier. Instead, multiple mechanisms seem plausible for ozone decomposition: one initiated by hydroxide ions and a self-decomposition in the absence of hydroxide.

Results and Discussion

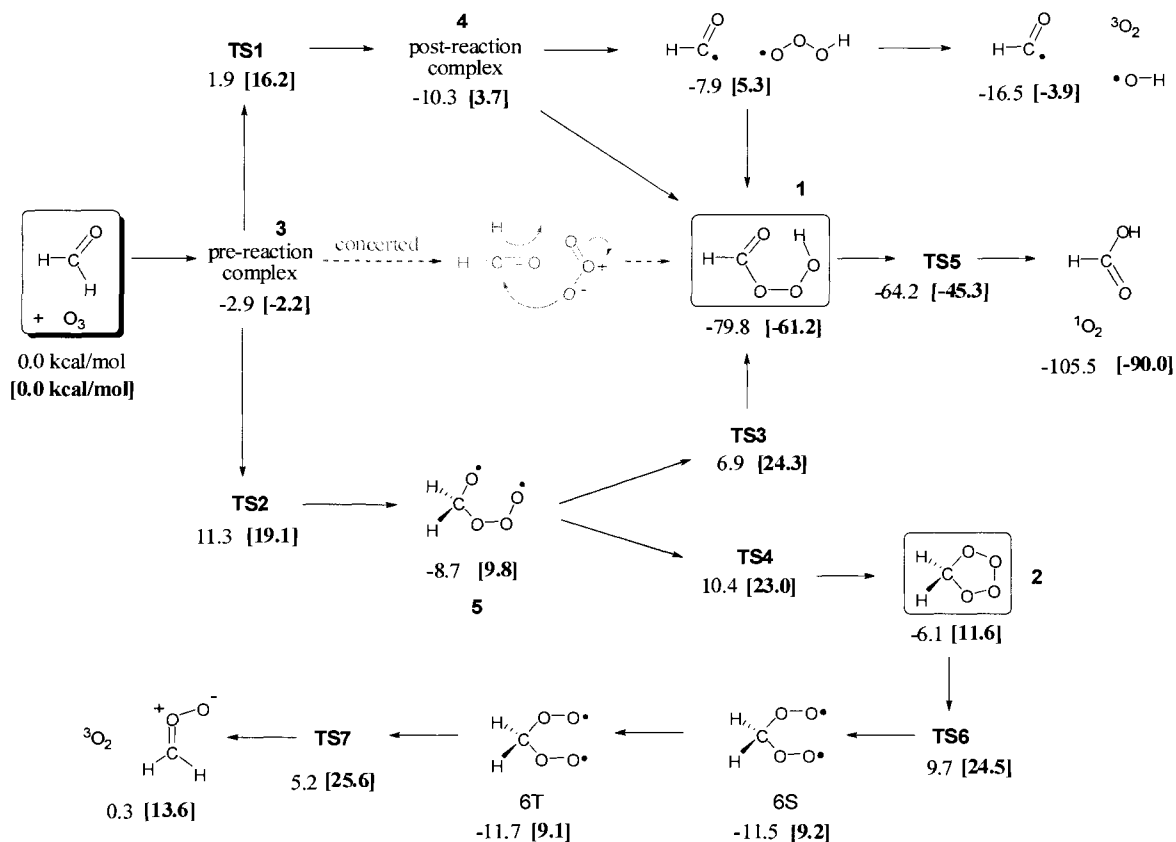
Formaldehyde + Ozone. Though appealing because of its simplicity, White and Bailey's concerted mechanism¹⁷ is inconsistent with many experimental results. Stepwise pathways can lead to a variety of intermediates. In the present study, the ozonation of aldehydes is modeled by the reaction of formaldehyde with ozone. Evidence for the existence of hydrotrioxides and tetroxolanes as intermediates suggests two major pathways in the reaction of formaldehyde with ozone (Scheme 1-4). First, ozone may abstract one of the two acyl hydrogens to produce an acyl radical and a hydrotrioxy radical, which can recombine to yield a hydrotrioxide (1). Second, ozone can add to the carbonyl carbon to give a diradical, a singlet by necessity, that can close to a tetroxolane (2). These two pathways are connected by an intramolecular hydrogen abstraction that could occur after addition to form hydrotrioxide 1.

Scheme 1-4. The two likely reaction pathways in the ozonation of formaldehyde.



The reaction of ozone with formaldehyde was modeled with M05-2X¹⁰⁷ density functional theory, followed by single point CCSD(T) calculations (Scheme 1-5). Formaldehyde and ozone first come together in a pre-reaction van der waals complex (3), predictably just slightly lower in energy than the two separated species. The geometry of this complex is favorable for both abstraction and addition. Relative CCSD(T) energetics and DFT geometries for the abstraction pathway are given in Figure 1-1.

Scheme 1-5. UM05-2X/6-311+G(d,p) [UCCSD(T)//UM05-2X] energetics for the two pathways in the oxidation of formaldehyde by ozone.



Following hydrogen abstraction (TS1), the acyl and hydrotrioxy radicals settle into a second van der waals complex (4), which favorably undergoes radical recombination to yield the hydrotrioxide (1). In a higher energy step, the fragile hydrotrioxy radical can fragment to give triplet oxygen and the hydroxy radical. Recombination is energetically much more favorable, being exothermic by 61.2 kcal/mol. The hydrotrioxide can also rearrange to formic acid and singlet molecular oxygen by TS5. Though DFT calculations suggest an abstraction barrier of just 1.9 kcal/mol, the correlated CCSD(T) method predicts a more substantial barrier of 16.2 kcal/mol, more consistent with the recent report by Yang and coworkers²⁷ and with experimental kinetic data. Braslavsky and Heicklen (1976) reported a rate constant of $2.1 \times 10^{-24} \text{ cm}^3$

molecule⁻¹ s⁻¹ for the reaction of formaldehyde and ozone,⁵⁶ much too small to correspond to a barrier of 1.9 kcal/mol. Therefore the energy profile for this reaction is better described by CCSD(T) methods than DFT. The large discrepancy between methodologies is most likely due to spin contamination in the DFT calculations.

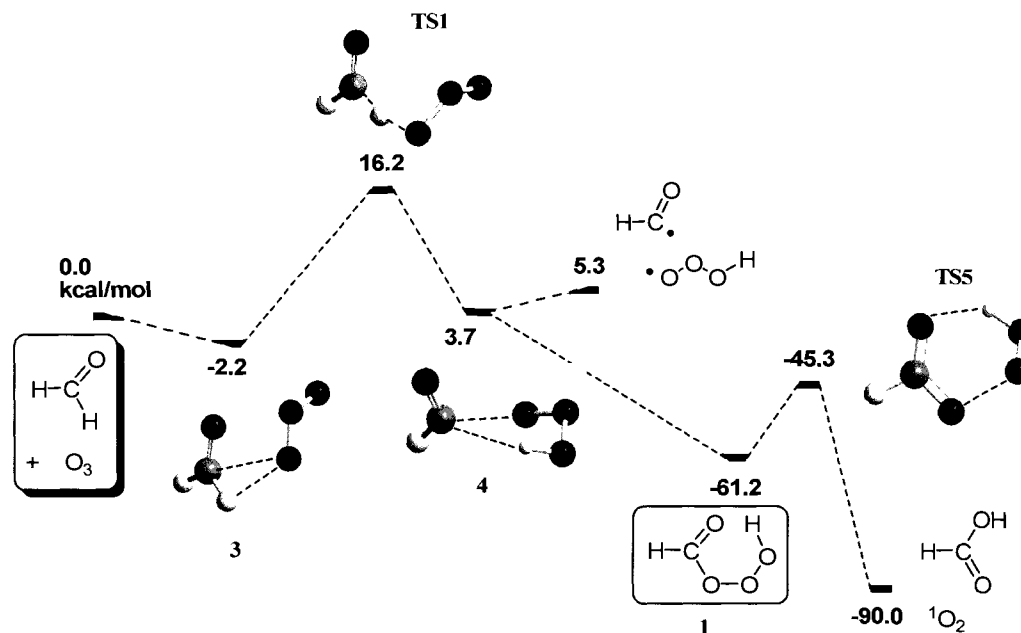


Figure 1-1. UCCSD(T)//UM05-2X energetics and UM05-2X/6-311+G(d,p) geometries for the abstraction pathway in the ozonation of formaldehyde.

Relative CCSD(T) energetics and DFT geometries for the addition pathway are given in Figure 1-2. Addition across the carbonyl double bond is predicted to be slow and stepwise. Ozone first adds to the carbonyl carbon by **TS2** and the resulting diradical (**5**) closes by **TS4** form a tetroxolane (**2**). Diradical **5** can also undergo an intramolecular hydrogen abstraction through **TS3** to form hydrotrioxide **1**, serving as the connection between the addition and abstraction pathways. Closure to the tetroxolane through **TS4**, however, is more favorable since the barrier is slightly lower. The tetroxolane can fragment across the O2-O3 bond by **TS6**, yielding a new singlet diradical (**6S**). Spin inversion yields a triplet diradical (**6T**), which can lose triplet oxygen through **TS7** to

form a carbonyl oxide, thus linking this pathway to Criegee chemistry. In contrast to the abstraction energy profile, where the overall trend is markedly downhill in energy, the addition profile is relatively horizontal, showing no substantial change in total energy after the addition transition state. This suggests that the tetroxolane could also serve as an intermediate in the formation of ozone from carbonyl oxides and molecular oxygen.

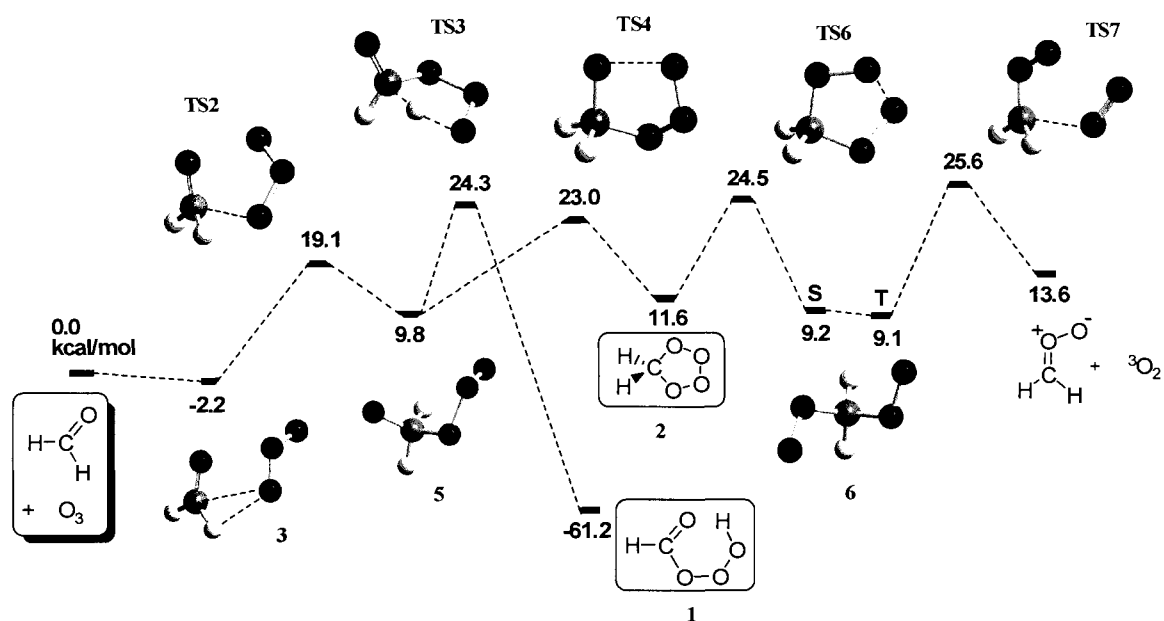
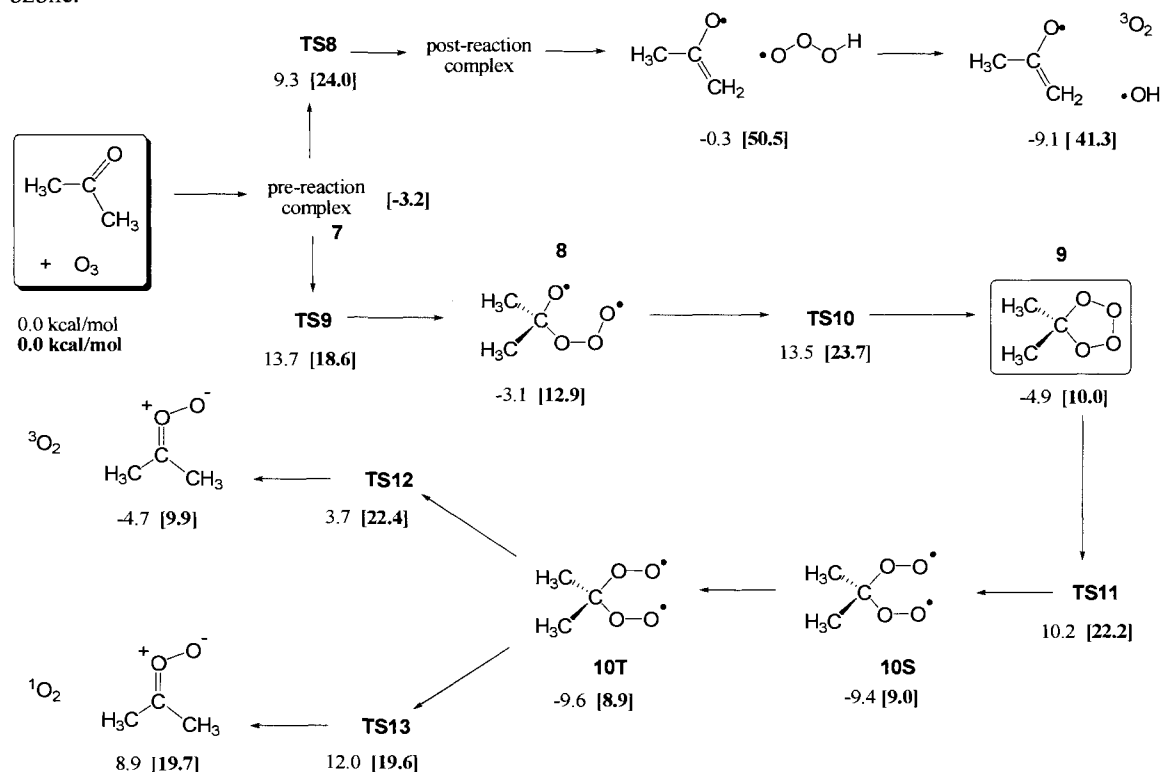


Figure 1-2. UCCSD(T)/UM05-2X energetics and UM05-2X/6-311+G(d,p) geometries for the addition pathway in the ozonation of formaldehyde.

Acetone + Ozone. The reaction of ozone with acetone can proceed by a similar addition or abstraction pathway and was modeled by CCSD(T)//DFT methods (Scheme 1-6). The pre-reaction van der waals complex (7) is similar to the ozone-formaldehyde complex, also having a favorable geometry for both addition and hydrogen abstraction.

Scheme 1-6. UM05-2X/6-311+G(d,p) [UCCSD(T)//UM05-2X] energetics for the oxidation of acetone by ozone.



Like formaldehyde, ozone can add to acetone in two steps, first adding to the carbonyl carbon (TS9), followed by closing of the diradical (8) through TS10 to a dimethyl tetraoxolane (9). This tetraoxolane can also open across the O2-O3 bond by TS11 to form a new singlet diradical (10S). Spin inversion to 10T and cycloreversion can produce a carbonyl oxide and either triplet or singlet molecular oxygen through TS12 or TS13, respectively. This overall energy profile is also relatively flat, again suggesting that ozone may be produced from molecular oxygen and carbonyl oxides. These

computations support Konrad's earlier conclusion that ^{18}O label exchange occurs through a tetroxolane intermediate.²⁹

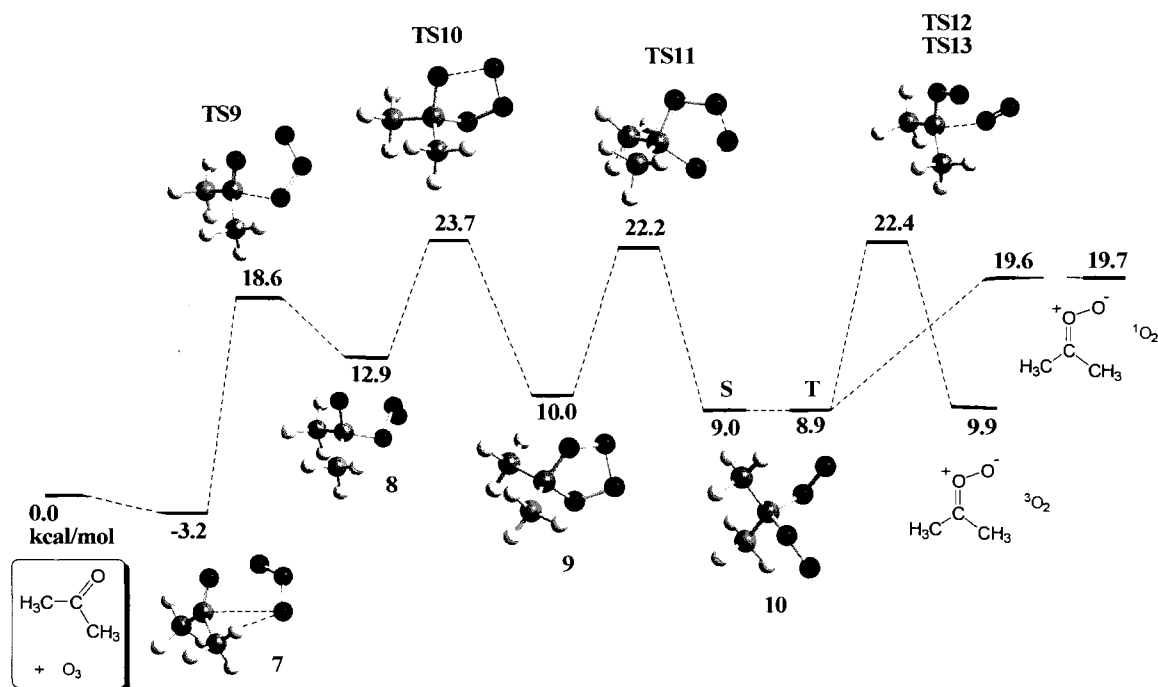


Figure 1-3. UCCSD(T)//UM05-2X energetics and UM05-2X/6-311+G(d,p) geometries for the addition pathway in the ozonation of acetone.

Hydrogen abstraction proceeds differently since ozone must abstract a methyl hydrogen atom, leading to delocalized radical 11 and the hydroperoxy radical, which fragments to the hydroxy radical and triplet oxygen. Hydrogen abstraction has a barrier of 27.2 kcal/mol and is endothermic by 14.4 kcal/mol. These energetics are consistent with those obtained by Yang et al. in the study of acetaldehyde ($E_a = 35.4$ kcal/mol, $\Delta E_R = 18.2$ kcal/mol).²⁷

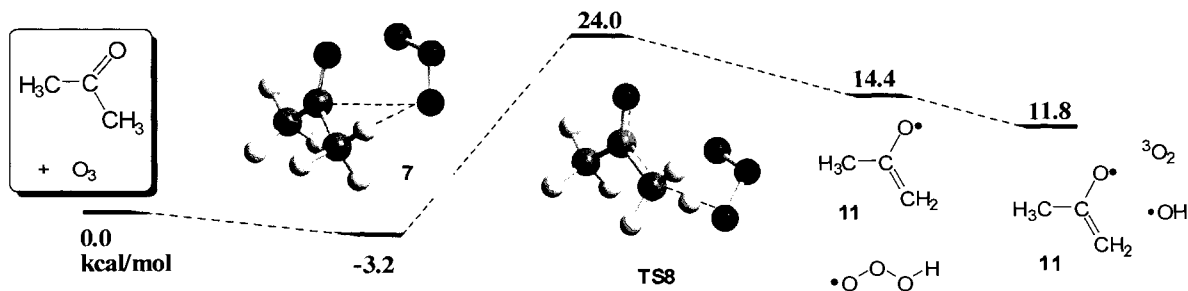
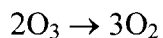


Figure 1-4. UCCSD(T)//UM05-2X energetics and UM05-2X/6-311+G(d,p) geometries for the abstraction pathway in the ozonation of acetone.

Bimolecular Ozone Decomposition. Two ozone molecules may come together in a simple bimolecular process to yield three oxygen molecules. This reaction was studied by CCSD(T)//B3LYP¹⁰⁸ methods (Figure 1-5).



As the two ozones approach, the overall dimeric structure has increasing open-shell character until the transition state is reached. Past the transition state, the overall structure has decreasing open-shell character. At the transition state, $S^2 = 0.99$, but at the reactants and products, $S^2 = 0$. During the reaction, a bond forms between the two ozones as the two adjacent bonds break, resulting in three oxygen molecules. An intrinsic reaction coordinate calculation confirmed this process. To balance the overall spin, this reaction must produce two triplet molecular oxygens of opposite spin and one singlet oxygen. This was verified by plotting the spin density (Figure 1-6), which shows the triplet oxygens on the ends, and singlet oxygen in the middle. Here, red and blue represent opposite spin.

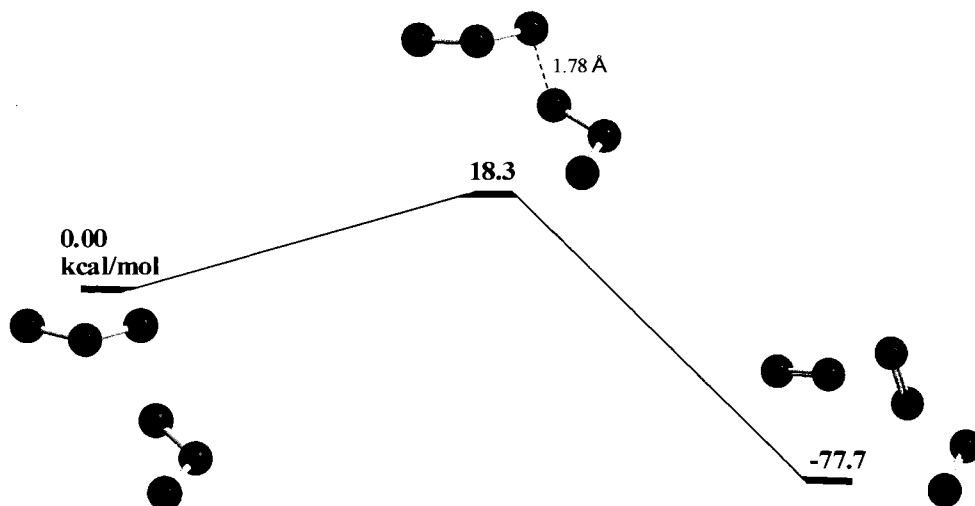


Figure 1-5. UCCSD(T)//UB3LYP energetics and UB3LYP/6-311+G(d,p) geometries for the bimolecular decomposition of ozone.

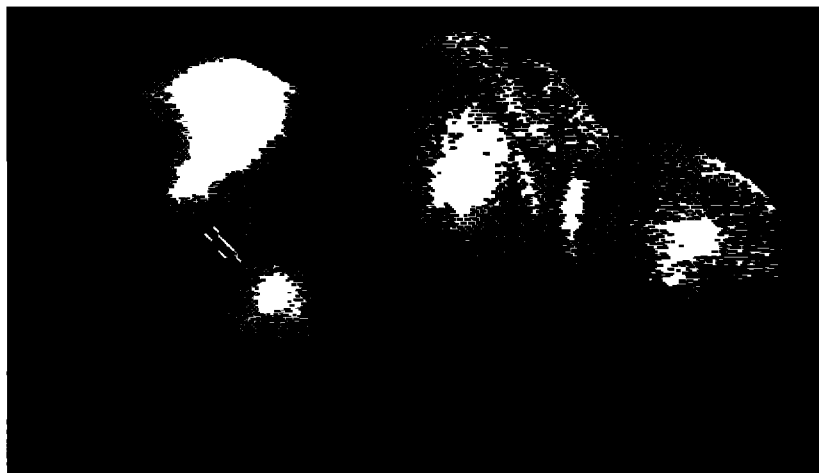


Figure 1-6. Spin density at UB3LYP/6-311+G(d,p) showing two triplet oxygens of opposite spin, one red and the other blue, and one singlet oxygen resulting from the bimolecular decomposition of ozone.

A similar transition state was proposed by Nakajima and Lin in 2003, but was only characterized by AM1 methods.³⁵ As a result, their calculated barrier of 35.9 kcal/mol is likely too high and their conclusion that this process is irrelevant is erroneous. The solution reported here is attractive in its simplicity and matches almost exactly the experimental activation energy reported by Ershov and Morozov.⁵⁴ These results are also in excellent agreement with the activation energy for the thermal decomposition of ozone

reported by Pshezhetskii et al. in 1959, 18.5 kcal/mol,⁵⁷ and by Glissmann and Schumacher in 1933, 30 kcal/mol.⁵⁸

To evaluate this reaction in an aqueous environment, energetics were also computed at the UB3LYP/6-311+G(d,p) level of theory with PCM¹⁰⁹ solvation and water as the solvent. A comparison of DFT, CCSD(T)//DFT, and DFT + PCM reaction energetics in kcal/mol is presented in Table 1.

Table 1. Comparison of calculated activation energies and exothermicities at different levels of theory for the bimolecular decomposition of ozone.

	UB3LYP/6-311+G(d,p)	UCCSD(T)// UB3LYP/6-311+G(d,p)	UB3LYP/6-311+G(d,p) + PCM (water)
E _a	2.7	18.3	5.0
ΔE _R	-86.0	-77.7	-82.8

The overall exothermicity predicted for this reaction at each level of theory is incorrect. For comparison, calculation with standard NIST heats of formation gives ΔE_R = -45.7 kcal/mol. Further calculations, perhaps UCCSD(T)//UB3LYP/6-311+G(d,p) + PCM (water), are needed to more accurately describe the overall energetics of this reaction.

Conclusions

In contrast to the concerted and highly exothermic reaction with alkenes, reactions of ozone with carbonyl compounds are slow, stepwise, and endothermic. There are two competitive pathways in the reaction of ozone with formaldehyde: acyl hydrogen atom abstraction, and stepwise addition across the carbonyl double bond. Acyl hydrogen atom abstraction produces an acyl radical and a hydrotrioxy radical. These can then recombine to give a hydrotrioxide, which may rearrange to formic acid and singlet oxygen, which is very favorable energetically. Addition across the carbonyl double bond first yields a singlet diradical, which closes to give a tetroxolane. This tetroxolane can open to a new diradical, which can lose molecular oxygen to form a carbonyl oxide. The two pathways are connected by an intramolecular hydrogen abstraction. Both the hydrotrioxide and tetroxolane are important intermediates in this reaction.⁵⁹

In the ozonation of acetone as a model ketone, there is similarly an addition and an abstraction pathway. In this case, abstraction of the alpha hydrogen has a higher barrier than acyl abstraction of formaldehyde. Consequently, addition is likely the dominant pathway. As with formaldehyde, ozone adds to the carbonyl carbon and the resulting diradical closes to a tetroxolane. This tetroxolane can open and lose either singlet or triplet molecular oxygen to form a carbonyl oxide. Since addition is favored over abstraction, the dimethyl tetroxolane is believed to be the key intermediate in the ozonation of acetone. Formation of the tetroxolane should be reversible, consistent with Konrad's observation of ¹⁸O label exchange.²⁹

For both formaldehyde and acetone, the energy landscape for the addition pathway is relatively flat. There is little change in overall energy after the addition

transition state is passed. This could indicate that tetroxolanes may also serve as intermediates in the *formation* of ozone from carbonyl oxides and molecular oxygen. Since both addition pathways are endothermic, the reverse process is exothermic.

Ozone decomposition can be described by a simple bimolecular process where two ozones meet and immediately fragment to three molecular oxygens: two triplets of opposite spin and a singlet. This is a self-destruction of ozone, rather than a process catalyzed or initiated by hydroxide ions. Self-annihilation may also be an important decomposition mechanism at in water at neutral pH, where hydroxide ion concentration is low at $10^{-7} M$. Though the activation energy calculated with CCSD(T)//DFT methods matches the experimental activation energy reported by Ershov and Morozov,⁵⁴ the predicted exothermicity does not agree with standard thermodynamic data. Additional calculations are needed to better represent the relative energies of the reactants and products. Further work is also needed to evaluate and clarify the role this reaction may play in aqueous solutions. This reaction is absent from the many kinetic models of ozone decomposition³⁰⁻⁵⁴ and may necessitate a reevaluation of these schemes.

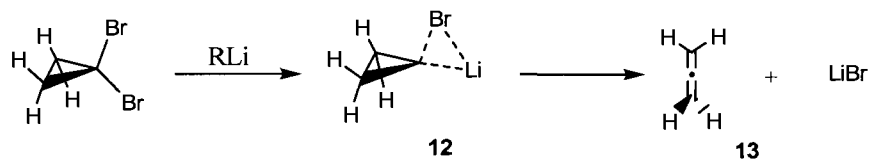
CHAPTER II

THE DOERING-MOORE-SKATTEBØL REARRANGEMENT

Introduction

The Doering-Moore-Skattebøl Rearrangement, named for the three chemists who independently discovered it in the early 1960s, is widely used in synthetic chemistry to form allenes, cumulenes, and strained ring systems. In this reaction, dihalocyclopanes undergo lithium-halogen exchange when treated with an alkyllithium to produce carbenoids, which undergo electrocyclic ring opening to allenes.

Scheme 2-1. The Doering-Moore-Skattebøl Rearrangement.



The connection between dihalocyclopanes and allenes was first reported in 1958 when Doering and LaFlamme treated dibromocyclopanes with sodium on alumina to yield allenes⁶⁰ (Figure 2-1(a)). Moore and Ward similarly obtained allenes, but with alkyllithiums.⁶¹⁻⁶³ Skattebøl studied this reaction in detail and applied it toward the synthesis of cyclic allenes and cumulenes⁶⁴⁻⁶⁷ (Figure 2-1(b)). The stereochemistry of this reaction was reported by Cope et al. in 1970, who synthesized (*R*)-(+)-1,2-cyclononadiene from optically active (*R*)-(-)-*trans*-cyclooctene⁶⁸ (Figure 2-1(c)).

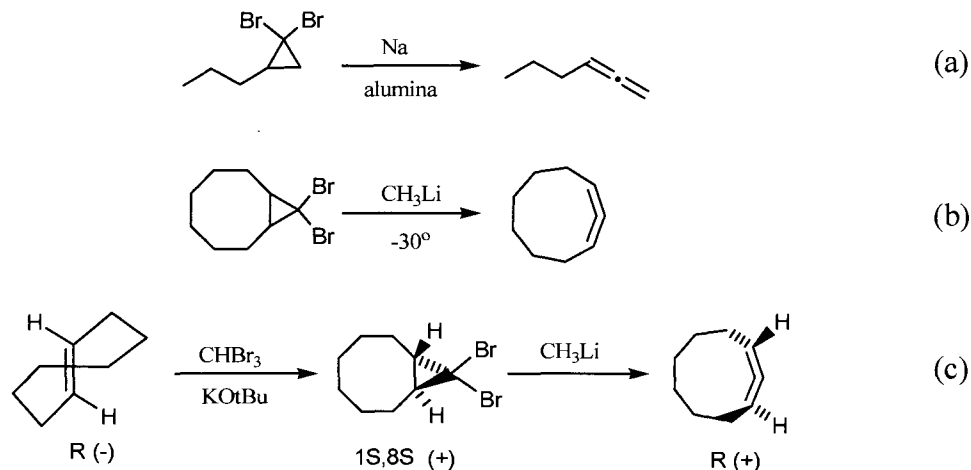


Figure 2-1. Historical milestones in the Doering-Moore-Skattebøl Rearrangement.

Carbenoids have been described by Closs and Moss in 1964 as “intermediates which exhibit reactions qualitatively similar to those of carbenes without necessarily being free divalent species.”⁶⁹ There have been several reports of two predicted carbenoid structures for 1-bromo-1-lithio-cyclopropanes (Figure 2-2): one with triangular C-Li-Br geometry (**12**), and a second with linear C-Li-Br geometry (**14**).⁷⁰⁻⁷⁷ The triangular structure is predicted to be of slightly lower energy. Dimers and other aggregates of carbenoids have been explored,⁷⁵⁻⁷⁷ but ring opening of these structures has not yet been characterized.

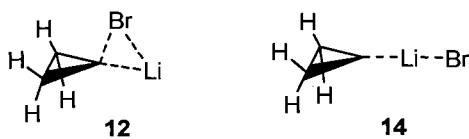
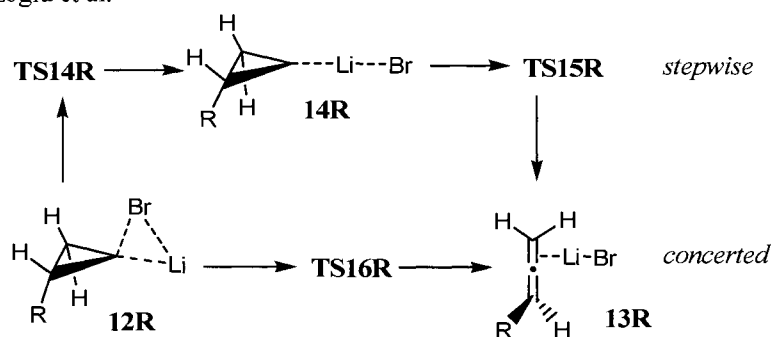


Figure 2-2. Triangular and linear geometries for lithium-bromine carbenoids.

Several experimental and computational studies have been reported for this basic reaction.⁷⁸⁻⁸⁰ Most recently, Azizoglu et al. located both minima and proposed two pathways from carbenoid **12R** to the allene **13R** (Scheme 2-2): a concerted mechanism for direct ring opening of **12R**, and a stepwise mechanism where **12R** first linearizes to

14R and then opens to allene **13R**.⁸⁰ Their main focus, however, was the effects of polar substituents (R) on the overall energetics. They find that electron donating groups lower the reaction barrier, suggesting cationic character at the carbenoid carbon. Though they propose this scheme, they did not locate the direct ring opening transition state **TS16R** for R = H.

Scheme 2-2. Concerted and stepwise pathways from lithium-bromine carbenoid **12R** to allene **13R** proposed by Azizoglu et al.



Most studies treat the Doering-Moore-Skattebøl Rearrangement as a carbene reaction, noting that ring opening is similar to that of cyclopropylidene. Valtazanios and Ruedenberg have described the ring opening of cyclopropylidene as a coordinate that bifurcates at a valley-ridge inflection point (VRI).⁸¹⁻⁸⁴ They define a VRI not as a stationary point, but as a point on the surface where one eigenvector of the Hessian matrix has a zero eigenvalue. This eigenvector is orthogonal to the gradient and thus represents a reversal in the surface curvature orthogonal to the gradient. Other studies, notably by Basilevskii,⁸⁵⁻⁸⁷ have more rigorously defined a VRI.⁸⁸⁻⁹³ For cyclopropylidene, this point represents the reversal in the sense of rotation during ring opening, where the initially disrotatory motion becomes conrotatory. The two possible modes of conrotatory motion define the two pathways after the bifurcation.

Results and Discussion

In this work, the reactions of carbenoids have been studied by density functional theory using the B3LYP¹⁰⁸ functional, followed in some instances by single point CCSD(T) calculations (Scheme 2-3). As in previous studies,⁷⁰⁻⁷⁷ two minima for the carbenoid structure were located (Figure 2-3): one with triangular C-Li-Br geometry (**12**) and the other, slightly higher in energy, with linear C-Li-Br geometry (**14**). Interconversion of the two minima should be facile as the barrier through **TS14** is low and the linear minimum is very shallow.

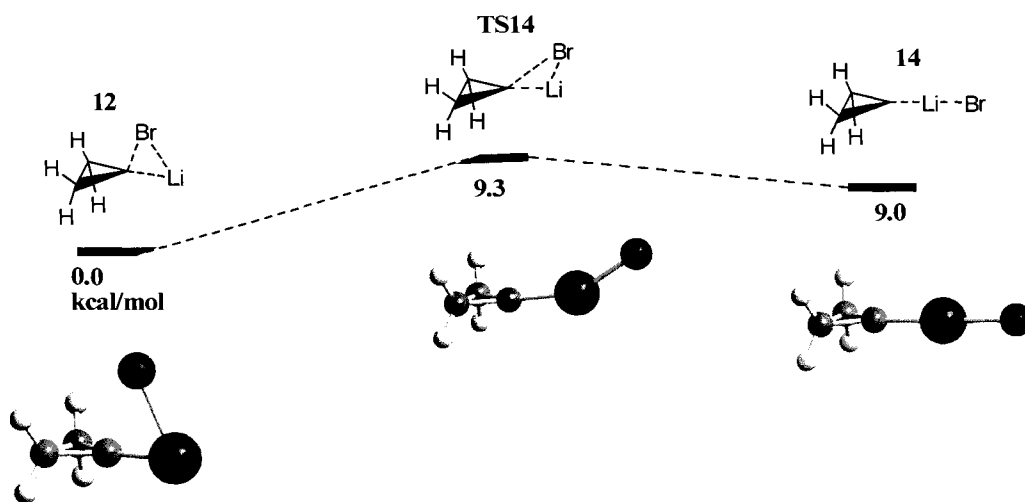


Figure 2-3. CCSD(T)//B3LYP/6-311+G(d,p) energies and geometries for the two carbenoid minima.

Each carbenoid structure can undergo ring opening to the same allene-LiBr complex (Scheme 2-3). The existence of two minima clearly defines two pathways from 1-bromo-1-lithio-cyclopropane (**12**) to the allene-LiBr complex (**13**). The overall energetics for this rearrangement were compared over several levels of theory, each of which predicts a similar energy profile (Table 2).

Scheme 2-3. CCSD(T)//B3LYP/6-311+G(d,p) energetics for the two pathways of the Doering-Moore-Skattebøl Rearrangement.

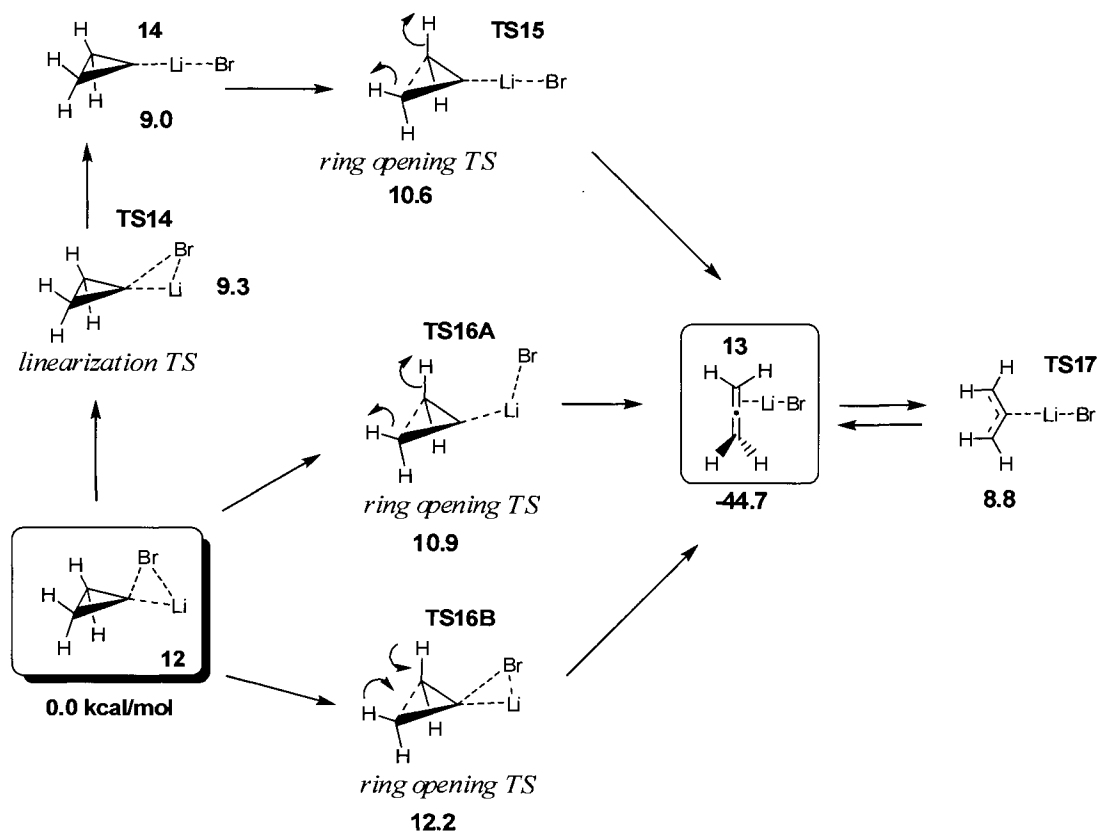


Table 2. Reaction energetics for the Doering-Moore-Skattebøl Rearrangement compared over several computational methods.

Structure	Erel ^(a) (kcal/mol)	Erel ^(b) (kcal/mol)	Erel ^(c) (kcal/mol)	Erel ^(d) (kcal/mol)
12	0.00	0.00	0.00	0.00
TS14	9.17	7.39	9.29	13.29
14	8.50	7.31	9.01	12.12
TS15	10.63	9.14	10.63	13.31
TS17	6.84	5.51	8.83	9.41
13	-44.71	-48.27	-44.69	-44.23
TS16A	11.75	9.45	10.86	13.80

(a) B3LYP/6-31+G(d), (b) B3LYP/6-311+G(d,p), (c) CCSD(T)//B3LYP/6-311+G(d), (d) MP2/6-31+G(d)

The bent carbenoid (**12**) can ring open immediately (**TS16A** or **TS16B**), or can first linearize (**TS14**) and then open (**TS15**). There is also a high energy planar transition state for rotation about the allene (**TS17**). Two geometrically distinct transition states

(**TS16A** and **TS16B**) exist with opposite modes of initial disrotatory ring opening of carbenoid **12**. In **TS16A**, lithium is slightly above the plane of the cyclopropyl ring, but in **TS16B**, both lie in the same plane. The C-Li-Br angle is the same in both structures at 118 degrees. The lower energy structure (**TS16A**) has the hydrogens *syn* to bromine rotating outward. This seems best explained by the proximity of bromine to the developing charge during ring opening. The carbenoid carbon is initially positively charged, but this charge is transferred to the terminal carbons as ring opening progresses. Since bromine is negatively charged, it better stabilizes this developing positive charge in **TS16A**, where bromine and the charge are in close proximity.

Direct ring opening of the bent structure has a modest barrier of approximately 10 kcal/mol, whereas the linear structure has an almost negligible barrier of just 2 kcal/mol. The net barriers, however, are nearly identical. This difference is attributed to the electronic nature of the carbenoid structures. Natural charge densities indicate that the carbenoid carbon of the linear structure is slightly positive, but negative in the bent structure (Figure 2-4). By the Woodward-Hoffmann rules, the cyclopropyl cation undergoes disrotatory opening and the cyclopropyl anion undergoes conrotatory opening. Since initial ring opening of both carbenoids is disrotatory, the linear structure should have a lower barrier to opening since its carbenoid carbon is has a slight positive charge. Due to its negatively charged carbenoid carbon, the bent structure must first undergo a charge reversal, which may be responsible for the higher barrier to ring opening.

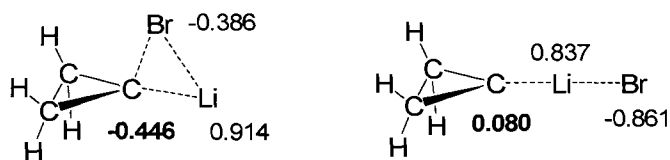


Figure 2-4. Natural charge densities at B3LYP/6-311+G(d,p) for the bent and linear carbenoids.

The intrinsic reaction coordinate (IRC) calculated from the bent ring opening transition state (**TS16A**) shows initial disrotatory motion and a modest decrease in energy, followed by a reverse in the sense of rotation to conrotatory motion and a steeper descent toward the allene (Figure 2-5). Conrotatory motion begins when the sense of rotation of one group reverses. Either sense of conrotatory motion can begin following the initial disrotatory ring opening, defining two enantiomeric pathways toward products. Since there are two rotating groups and either group can reverse direction, there must be two product minima on the potential energy surface.

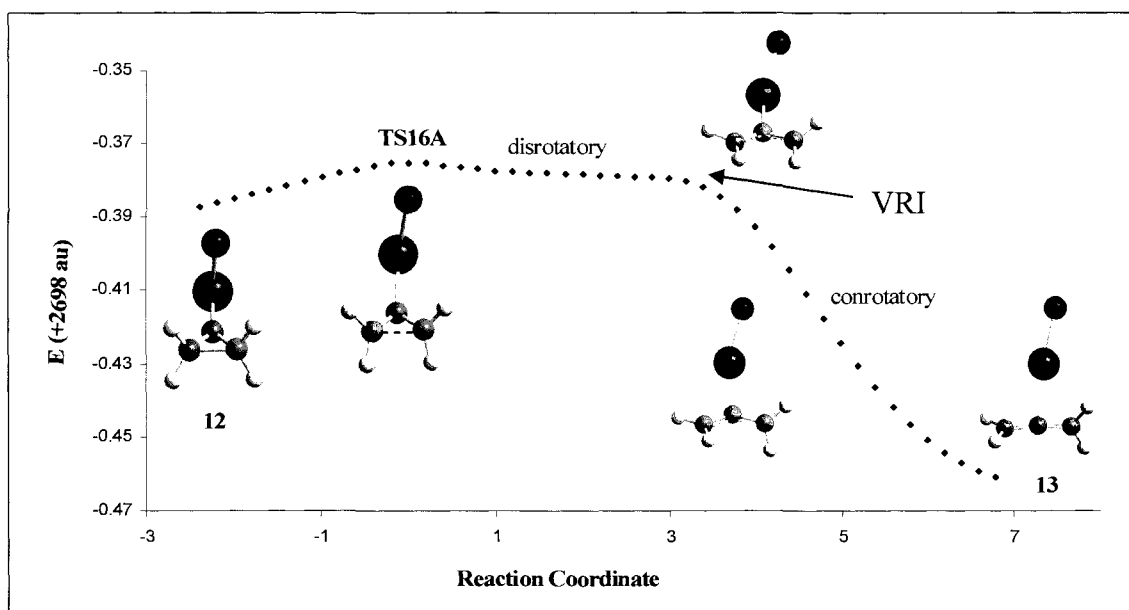


Figure 2-5. B3LYP/6-311+G(d,p) intrinsic reaction coordinate showing initially disrotatory ring opening followed by conrotatory ring opening in the Doering-Moore-Skattebøl Rearrangement.

The point on the surface at which the rotation reverses is a valley-ridge inflection (VRI) point, as described by Valtazanov and Ruedenberg.⁸¹⁻⁸⁴ A VRI is characterized as a point along the reaction path with zero curvature orthogonal to the gradient, when the sign of the surface curvature changes (Figure 2-6). The ring opening transition state is a saddle point, a local minimum on the surface, but a maximum along the reaction

coordinate. Following the direction of the gradient leads down the valley, which is becoming shallower, until the beginning of a ridge is reached. The direction of the gradient vector is now changed and the reaction path leads more sharply to products. For achiral carbenoids, these two product valleys will be of equal energy since the two possible allenes are identical. Asymmetrically substituted carbenoids, however, will have a different surface topology where one product valley will descend more steeply than the other. This presents the possibility that specific allene enantiomers can be synthesized by ring opening of specific chiral carbenoids.

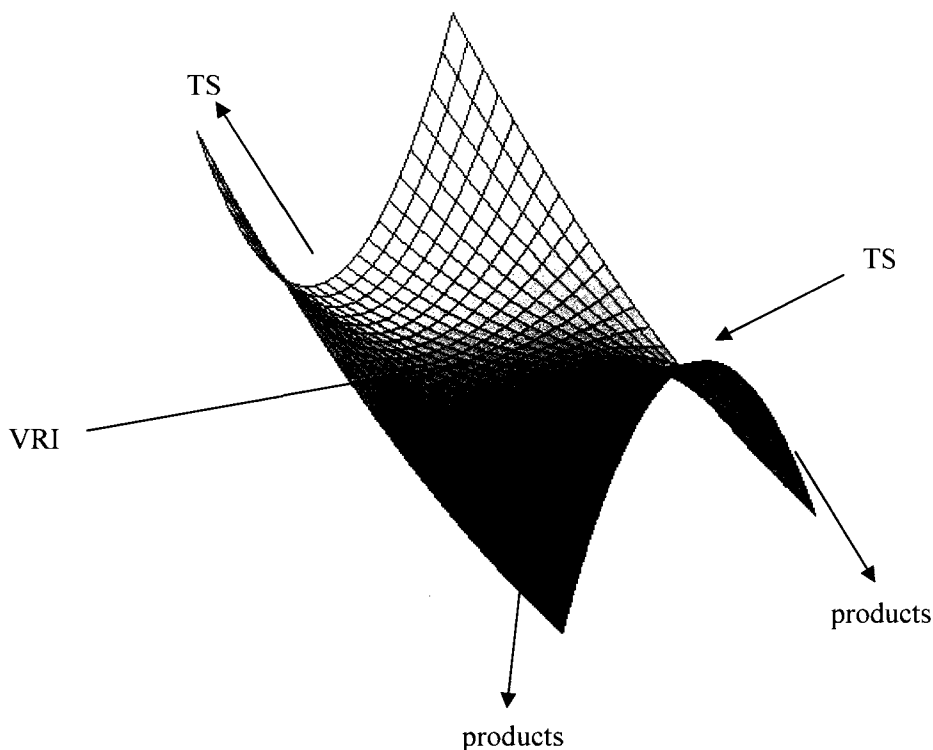
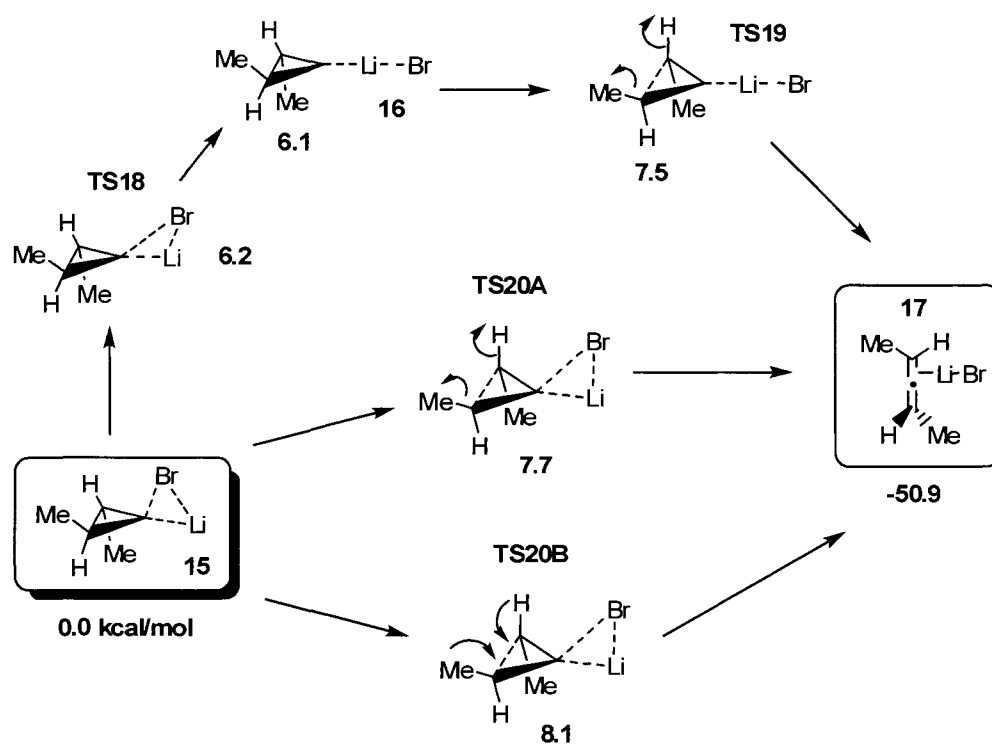


Figure 2-6. Sample topology of a valley ridge inflection point where the surface curvature changes. The test function depicted is $f(x,y) = yx^2 + 0.2y^2$.

Chiral Carbenoids. As Cope et al. showed,⁶⁸ chiral carbenoids open stereospecifically to chiral allenes, consistent with an asymmetric surface topology. A *trans*-dimethyl carbenoid such as **15** is the simplest chiral carbenoid to illustrate the stereochemistry.

Note that there exists only one bent carbenoid structure as the two initial bromines are homotopic. Not surprisingly, there are two carbenoid minima with triangular and linear geometries (**15** and **16**) with corresponding ring opening transition states (**TS19** and **TS20A/B**). Each ring opening transition state proceeds to *S*-2,3-pentadiene, as confirmed by IRC calculations. The energy profile is similar to the parent carbenoids (Scheme 2-4).

Scheme 2-4. B3LYP/6-311+G(d,p) energetics for the formation of *S*-2,3-pentadiene (**17**) from *trans*-1-bromo-2,3-dimethyl-1-lithiocyclopropane (**15**).



The IRC for the ring opening of the bent structure (**15** through **TS20A**, Figure 2-7) follows the same stereochemistry as reported by Cope et al.⁶⁸ In contrast to the parent carbenoid, the dimethyl carbenoid does not show the same reversal in the sense of rotation along the reaction coordinate. As the coordinate approaches the valley-ridge inflection point, rotation of one group slows and stops, instead of reversing direction, while the other continues. Initially synchronous disrotatory ring opening becomes

asynchronous disrotatory at a valley-ridge inflection point. In this case, the VRI is the point at which one group stops rotating. Because chiral carbenoids trace stereospecific pathways to chiral allenes, it can be argued that these are not truly bifurcating surfaces since the two allene enantiomers are not produced with equal probability. Perhaps the coordinate is more appropriately described as an asymmetric bifurcation, indicating that two products exist, but that the path to one is more favored.

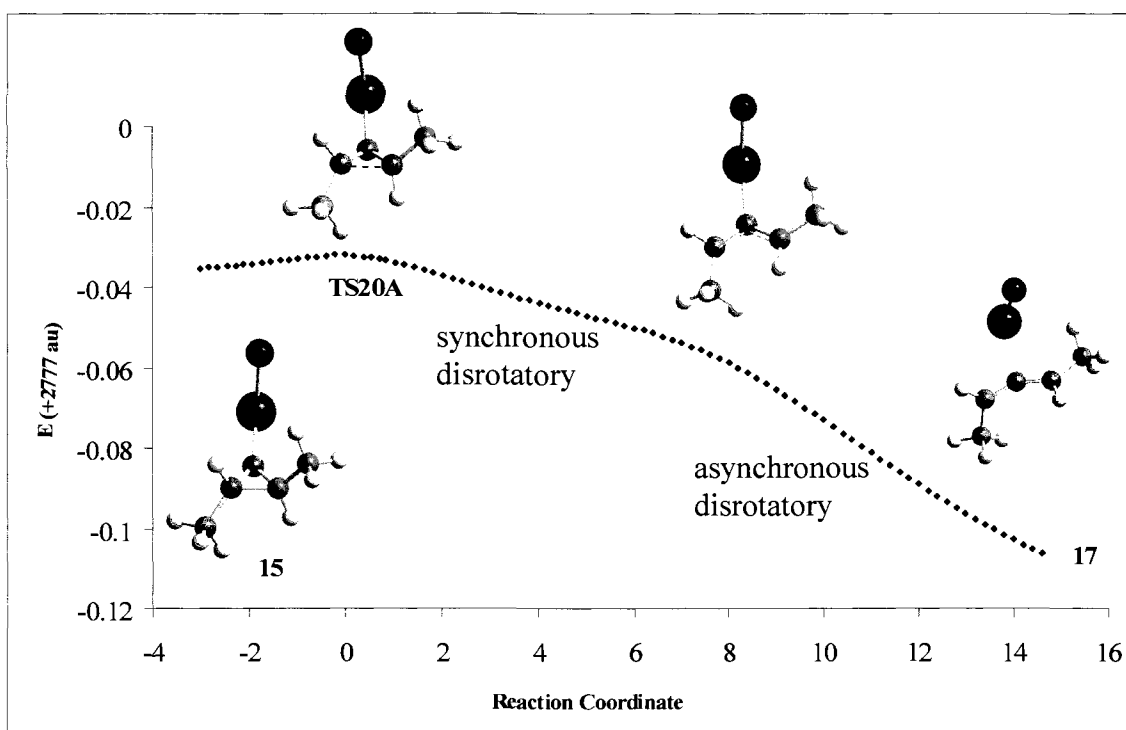


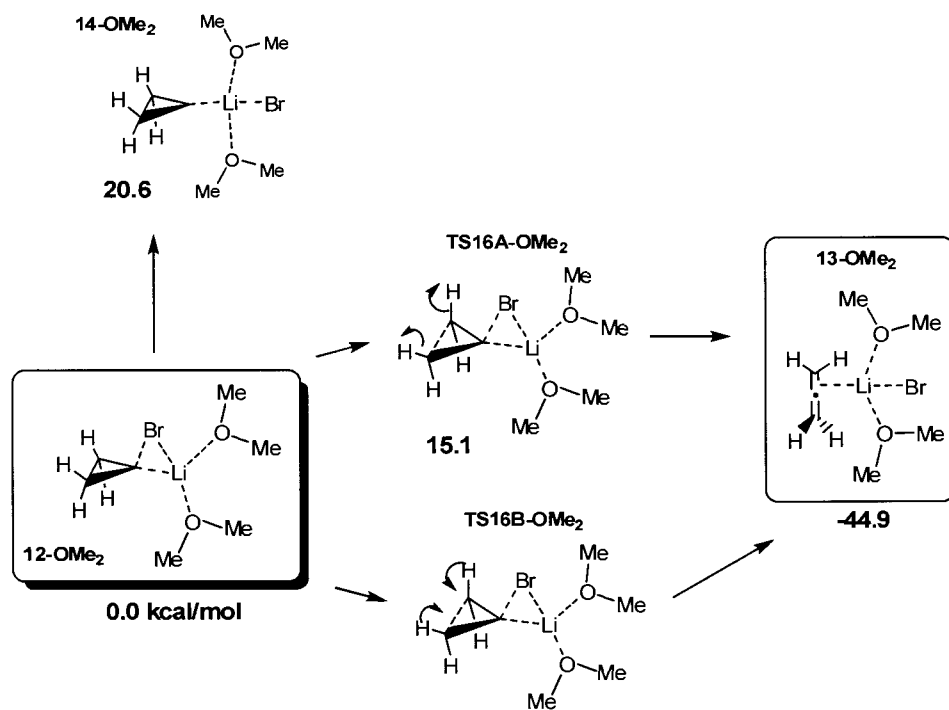
Figure 2-7. B3LYP/6-311+G(d,p) intrinsic reaction coordinate showing the disrotatory ring opening of *trans* dimethyl carbenoid **15** to yield *S*-1,2-pentadiene (**17**).

Reaction energetics were also computed using both explicit and implicit solvation models to better represent experimental reaction conditions. For the explicit solvation model, the carbenoid structures were complexed with two dimethyl ether molecules and optimized at the B3LYP/6-311+G(d,p) level of theory. Both the linear (**14-OMe₂**) and bent (**12-OMe₂**) minima exist under explicit solvation, but the linear structure jumps to 20.6 kcal/mol above the bent structure, compared with only 7.3 kcal/mol *in silico* at the

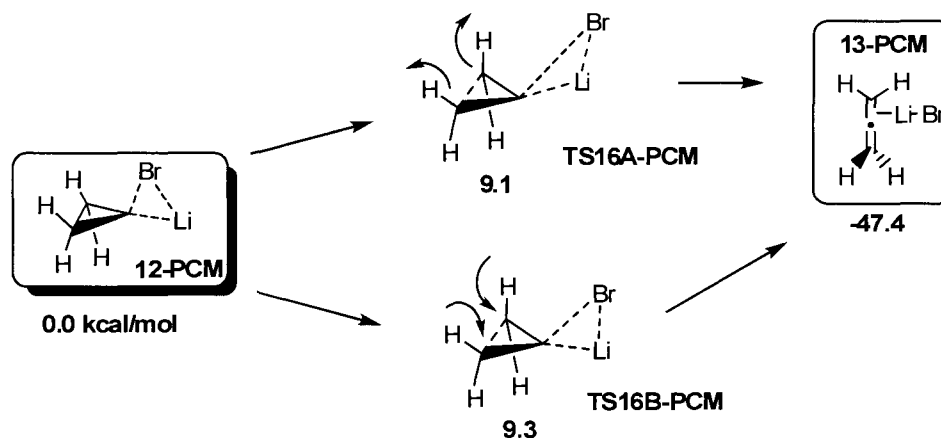
same level of theory. A transition state for ring opening of the linear structure (**TS15-OMe₂**) could not be located. The barrier for ring opening of the bent structure (**TS16A-OMe₂**) is slightly higher, but comparable in energy *in silico* (Scheme 2-5).

For the implicit model, stationary points were reoptimized with the Polarizable Continuum Model (PCM)¹⁰⁹ at B3LYP/6-311+G(d,p) and diethyl ether as the solvent. In this case, neither the linear structure (**14-PCM**) nor its corresponding ring opening transition state (**TS15-PCM**) could be located (Scheme 2-6).

Scheme 2-5. B3LYP/6-311+G(d,p) energetics for the parent carbenoid (**12-OMe₂**) explicitly solvated by complexation with two dimethyl ether molecules.



Scheme 2-6. Implicit solvation for the ring opening parent carbenoid (**12-PCM**) computed at B3LYP/6-311+G(d,p) with PCM solvation in diethyl ether.



Ring opening of the bent structure again has a low predicted barrier, comparable to the gas phase calculations. Overall, both solvation models favor the bent minimum (**12**) as the structure that ring opens with the hydrogens *syn* to bromine rotating outward (**TS16A**). The linear carbenoid (**14**) will likely not represent solution-phase reactions. *In silico*, the one- and two-step ring opening processes are competitive, but calculations including solvation predict that ring opening occurs in a single step.

Though commonly associated with cyclopropylidene chemistry, the Doering-Moore-Skattebøl Rearrangement must begin as a carbenoid. Following the initial lithium-halogen exchange to form a carbenoid, the exact timing of lithium bromide dissociation has remained unclear. To address this issue, the energy of LiBr dissociation was calculated at three points along the reaction path with PCM solvation in diethyl ether: at the starting bent carbenoid, at the transition state, and at the allene (Figure 2-8). Free energies were assessed at -30° C, a typical reaction temperature, and also with PCM

solvation. For the starting carbenoid, dissociation is unfavorable based on both the energy and free energy changes. For the allene, dissociation is favorable. This series indicates that LiBr dissociation should occur after the ring opening transition state is passed. There are no free carbenes present in this reaction.

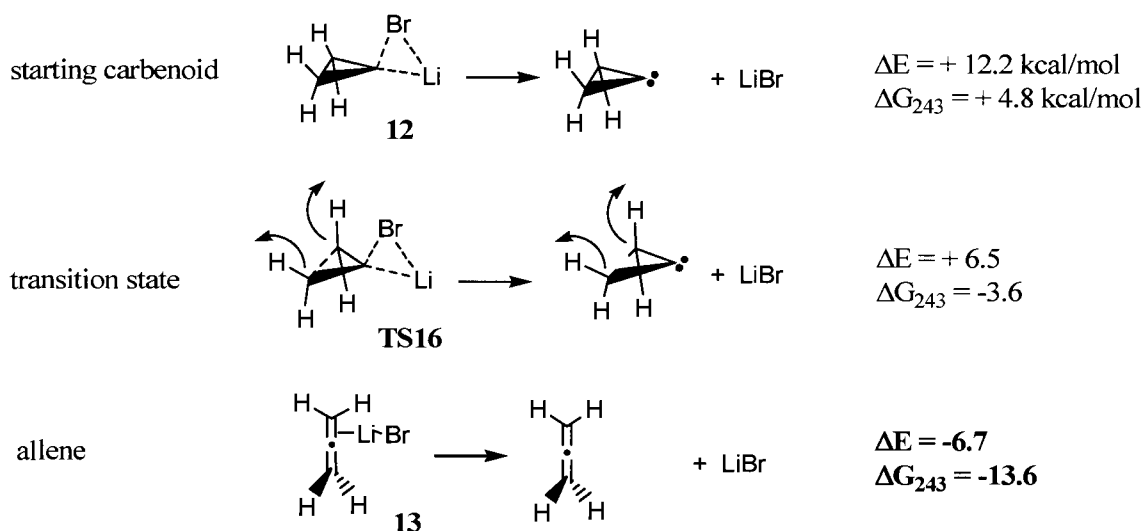
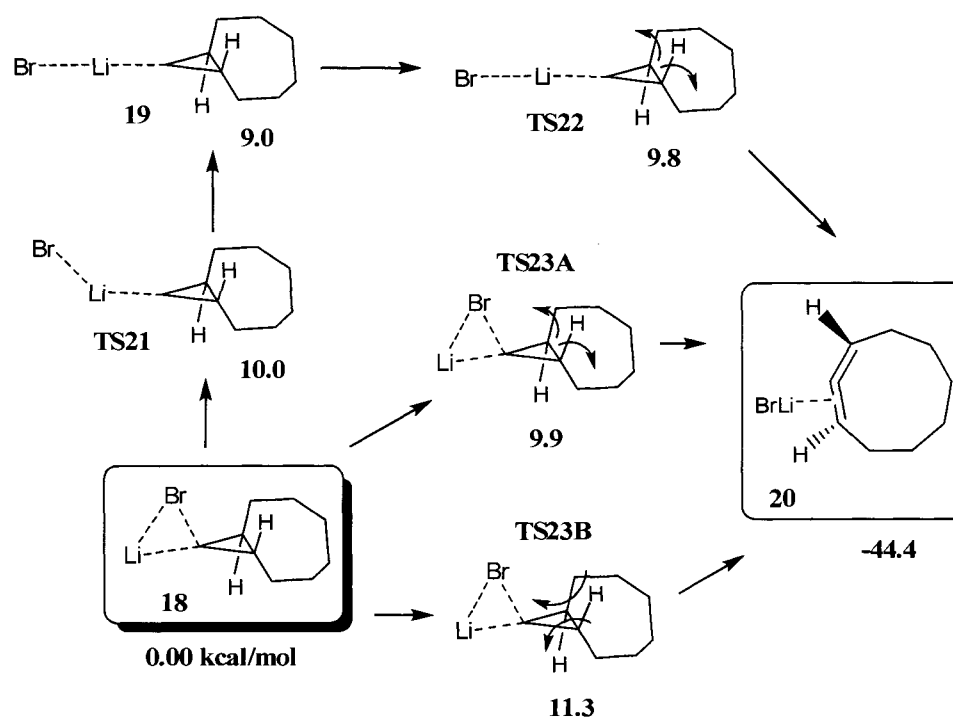


Figure 2-8. Dissociation energies and free energies at -30°C for the starting carbenoid (**12**), transition state (**TS16**), and allene (**13**) in the Doering-Moore-Skattebøl Rearrangement computed at B3LYP/6-311+G(d,p) with PCM solvation in diethyl ether.

Trans C9. This same model chemistry was applied to the formation of 1,2-cyclononadiene, a classic Doering-Moore-Skattebøl reaction⁶⁴⁻⁶⁸ (Scheme 2-7). Analogous to the *trans* dimethyl carbenoid, a *trans* bicyclic carbenoid (**18**) was considered. There are similarly two minima with bent (**18**) and linear (**19**) geometries, each of which can ring open to 1,2-cyclononadiene (**20**). Like the dimethyl carbenoids, there is only one bent carbenoid structure since the two initial bromines that could be exchanged with lithium are homotopic. There are two ring opening transition states (**TS23A** and **TS23B**) for bent carbenoid **18**. The lower energy structure (**TS23A**) again has the groups *syn* to bromine rotating outward. Overall reaction energetics are quite

similar to the parent and dimethyl structures. Since calculations with both a large and small basis set showed similar energetics for the parent carbenoid (Table 2), the smaller 6-31+G(d) basis set was used as a compromise of speed and accuracy for the larger molecules.

Scheme 2-7. B3LYP/6-31+G(d) energetics for the ring opening of *trans* bicyclic carbenoid **18** to (*R*)-1,2-cyclononadiene (**20**).



The IRC for ring opening of bent *trans* carbenoid (**18** through **TS23A**) follows a similar path as the dimethyl carbenoid, as it opens to a single enantiomer of 1,2-cyclononadiene, in this case *R* (**20**). Again, ring opening is initially disrotatory where both groups rotate synchronously, but one group slows and the other continues as the allene is formed (Figure 2-9). This ring opening of **18** follows a least-motion pathway where the hydrogens do most of the rotating while the ring remains essentially in place. This observation can be extended to other asymmetrically substituted chiral carbenoids to

predict the stereochemical outcome of ring opening. This phenomenon is similar in the ring opening of *trans*-dimethyl carbenoid **15** (Figure 2-6).

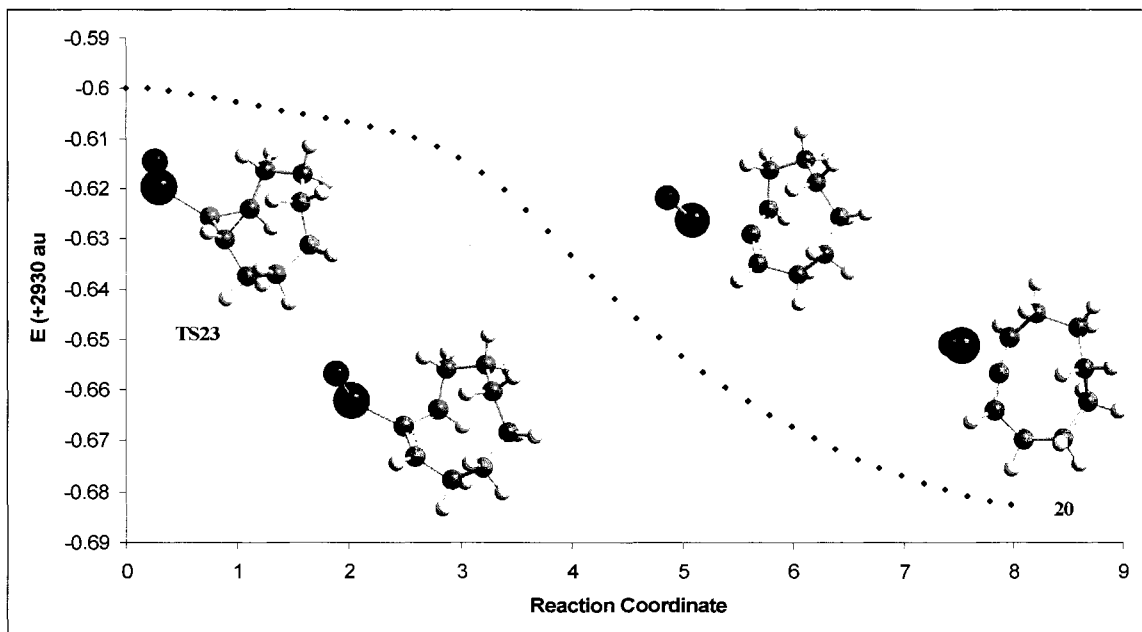
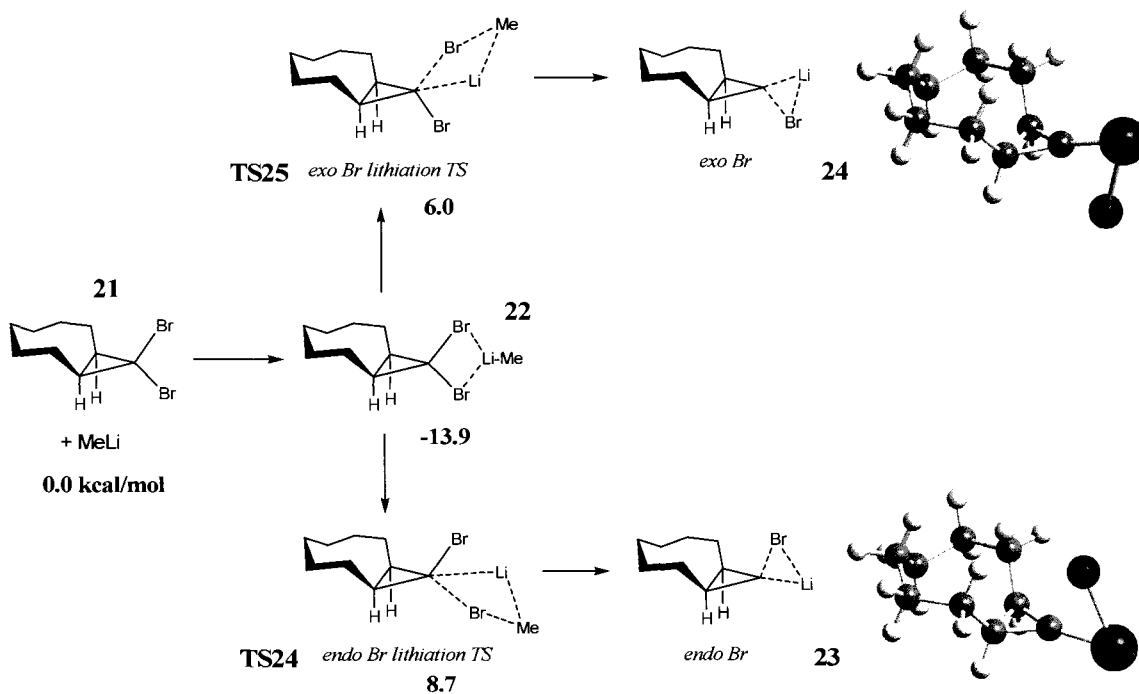


Figure 2-9. B3LYP/6-31+G(d) forward intrinsic reaction coordinate showing the disrotatory ring opening of *trans* bicyclic carbenoid **18** through **TS23A** to (R)-1,2-cyclononadiene (**20**).

Cis C9. Ring opening of a *cis* bicyclic carbenoid, however, is more complex. In *cis*-1,1-dibromobicyclo[6.1.0]nonane, the two bromines are diastereotopic. Either bromine can be exchanged with lithium to give two diastereomers for the bent carbenoid, described as *endo* (**23**) and *exo* (**24**) according to the orientation of bromine relative to the 6-carbon bridge. To determine which diastereomer is preferred, both lithiation transition states were located with methyllithium as the lithium donor. The two transition states are also labeled *endo* (**TS24**) and *exo* (**TS25**) according to which diastereomer is produced. There is a pre-reaction complex (**22**) that forms between methyllithium and 1,1-dibromobicyclo[6.1.0]nonane (**21**) where lithium sits equidistant from the two bromines. Accordingly, the geometry of this complex is favorable for exchange with either bromine

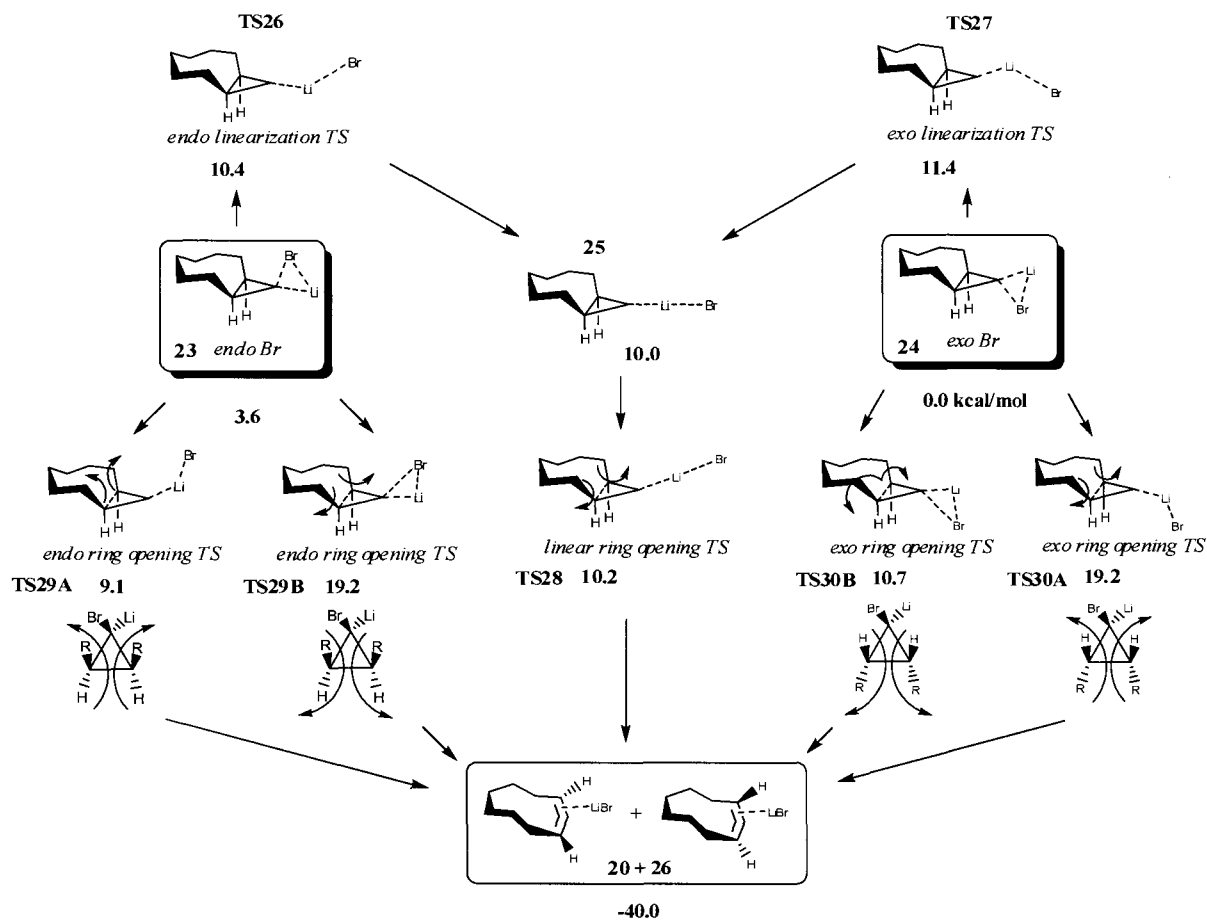
(Scheme 2-8). The *exo* lithiation (**TS25**) has a lower barrier and produces the more energetically favorable *exo* diastereomer (**24**, Scheme 2-9).

Scheme 2-8. B3LYP/6-31+G(d) energetics showing lithium-halogen exchange with the diastereotopic bromines in **21** to form two *cis* bicyclic carbenoids **23** and **24**.



Scheme 2-9 summarizes the results for ring opening of both carbenoids. Each diastereomer has a corresponding linearization (**TS26** and **TS27**) and two ring opening transition states (**TS29A/B** and **TS30A/B**). Both linearizations predictably lead to the same linear minimum (**25**), which also has a ring opening transition state (**TS28**). To more clearly illustrate the initial mode of disrotatory ring opening, the bromine face of the cyclopropyl ring is shown, where R represents the 6 carbon bridge.

Scheme 2-9 B3LYP/6-31+G(d) energetics for ring opening of the two *cis* bicyclic carbenoids **23** and **24**.



Both enantiomers of 1,2-cyclononadiene should be products of this reaction. Since both diastereomers are achiral, ring opening should yield a racemic mixture. For each diastereomer, the two direct ring opening transition states (**TS29A/B** and **TS30A/B**) markedly different energy. This difference is due to steric hindrance of the initial ring opening. The group *syn* to the bromine can open outward or inward. In each case, the lower energy transition state has the two sides of the ring rotating away from each other (**TS29A** and **TS30B**). When the cyclopropane ring opens in these transition states, the two sides of the ring rotate away from each other, leaving the two hydrogens on the underside to rotate toward each other. In the two remaining transition states (**TS29B** and

TS30A), the two hydrogens rotate away from each other and the two sides of the ring on the underside are forced to rotate toward each other. As a consequence, this ring opening is sterically disfavored, hence the much higher barrier.

Like the *trans* dimethyl (**15**) and *trans* bicyclic (**18**) carbenoids, both the *cis endo* (**23**) and *cis exo* (**24**) bicyclic carbenoids show the same synchronous-asynchronous disrotatory ring opening to 1,2-cyclononadiene. The IRC for the ring opening of the *cis exo* carbenoid (**24** through TS30A) is shown in Figure 2-10. Calculation of the IRC for ring opening of the *cis endo* carbenoid (**23**) was repeatedly unsuccessful.

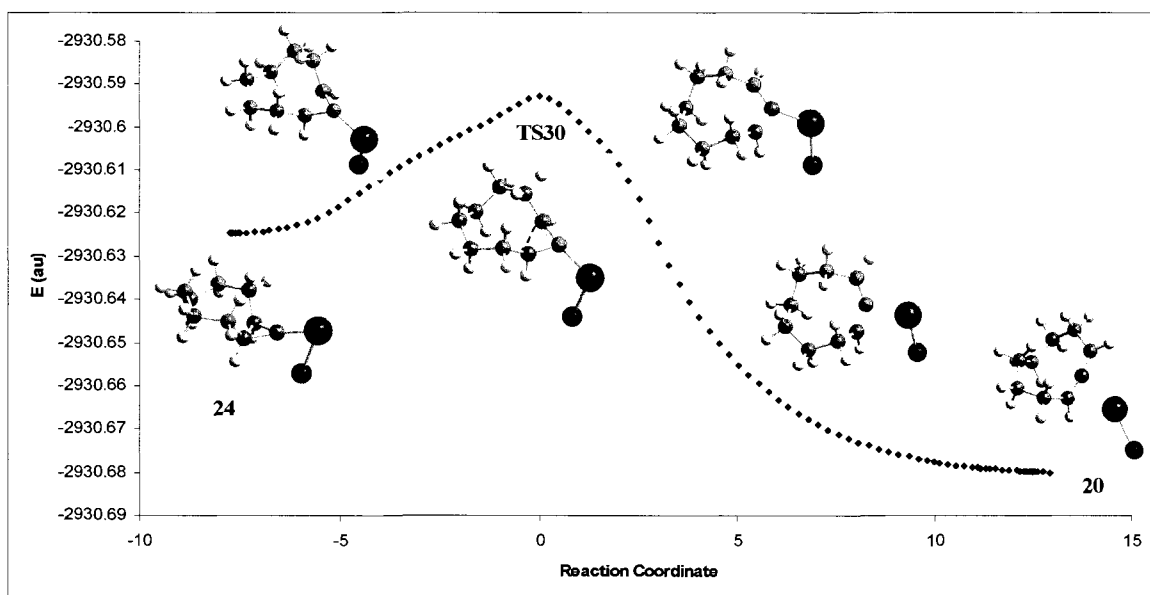
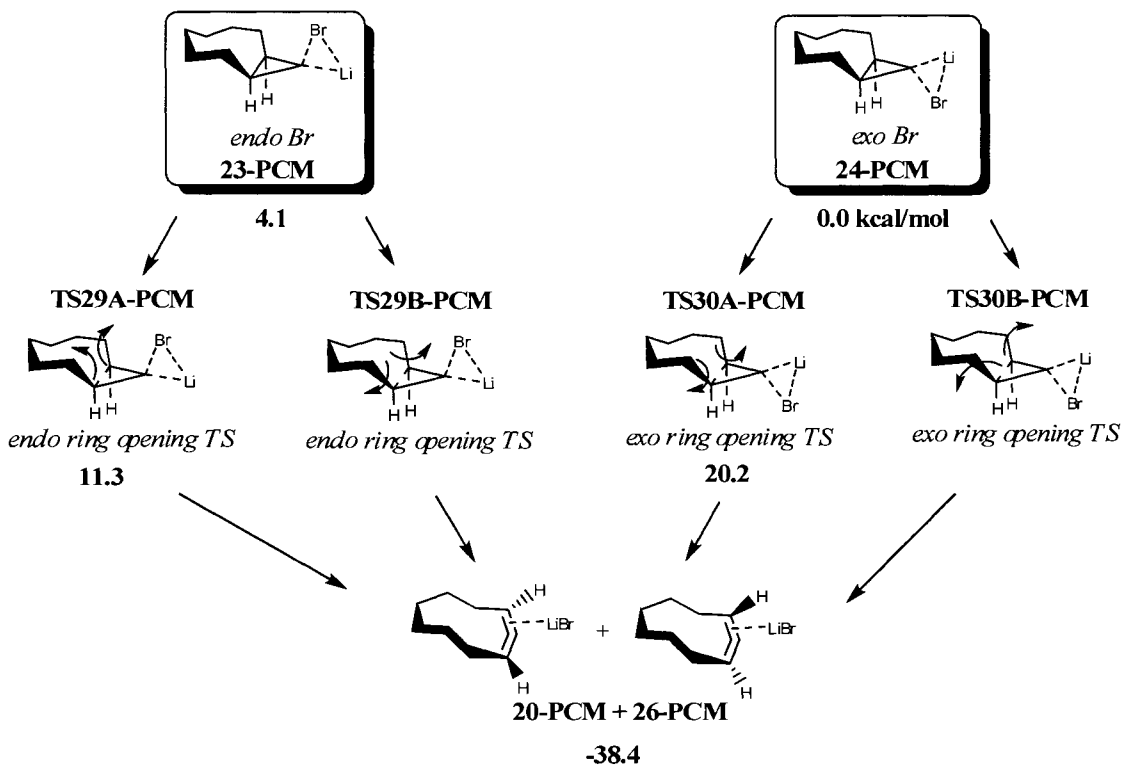


Figure 2-10. B3LYP/6-31+G(d) intrinsic reaction coordinate showing the disrotatory ring opening of carbenoid **24** through TS30A to (*R*)-1,2-cyclononadiene (**20**).

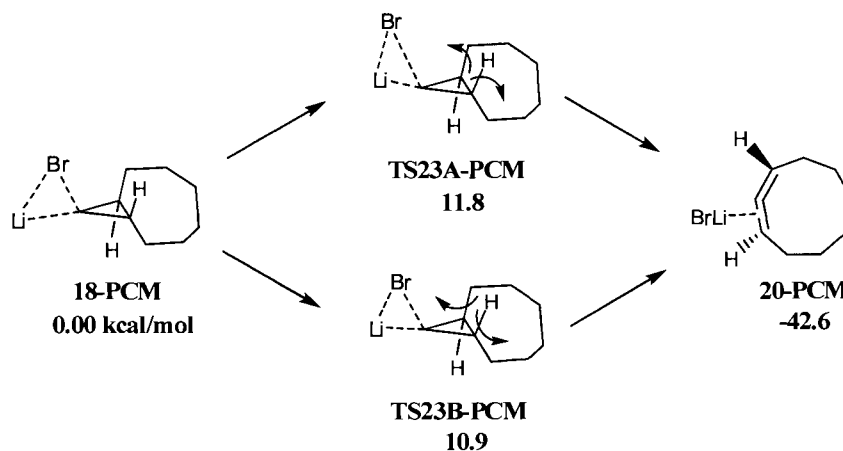
Implicit solvation models were also explored for the bicyclic carbenoids. The overall energetics parallel the *in silico* results, though the scheme is greatly simplified since the linear structures again do not exist. As with the parent structures, reoptimization with PCM solvation failed to locate either a linear minimum or its corresponding ring opening transition state. Again, single step ring opening of the bent

carbenoid is favored over linear ring opening. Including solvation does not significantly change the relative energies of the important structures in the scheme. For the *cis* bicyclic carbenoids, results with implicit solvation are summarized in Scheme 2-10. For the *trans* bicyclic carbenoids, results are summarized in Scheme 2-11. **TS29B-PCM** and **TS30B-PCM** have not yet been located, but their energies are predicted to parallel the *in silico* results.

Scheme 2-10. Implicit solvation for the ring opening of two *cis* bicyclic carbenoids **23-PCM** and **24-PCM** computed at B3LYP/6-31+G(d) with PCM solvation in diethyl ether.

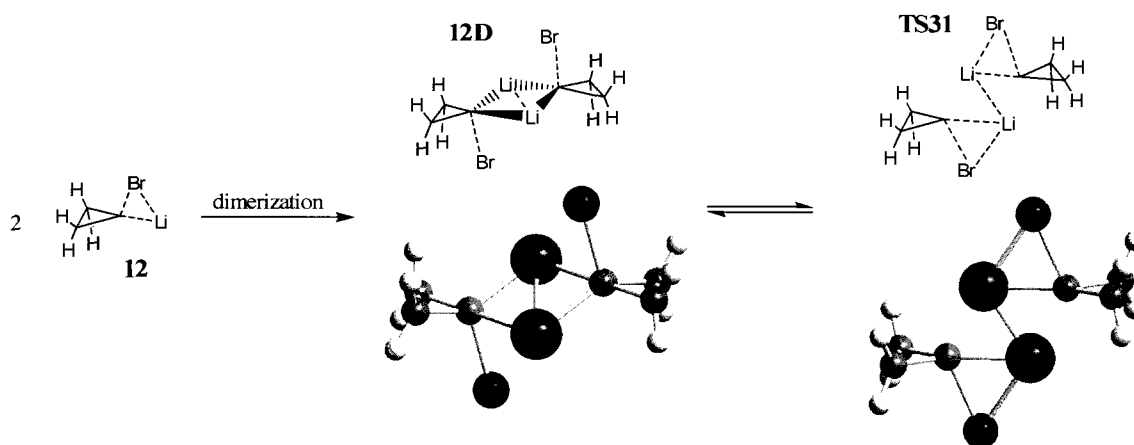


Scheme 2-11. Implicit solvation for the ring opening of *trans* bicyclic carbenoid **18-PCM** computed at B3LYP/6-31+G(d) with PCM solvation in diethyl ether.



Dimers. Many organolithium compounds are known to exist in solution as oligomers; so consequences of dimerization were explored for these cyclopropyl carbenoids. Dimer chemistry was modeled for the parent carbenoid (**12**). Two dimer structures were considered: one in which all bromines and lithiums are coplanar, and a second in which both LiBr groups are bent out of plane (Scheme 2-12). In both structures, each carbenoid carbon is complexed with two lithiums and one bromine, increasing its cationic character. The optimized structure for the planar dimer (**TS31**) shows a single imaginary frequency and may be best described as a transition state for the two monomers exchanging relative positions. This structure is easily optimized as a transition state *in silico*, but fails to optimize as either a minimum or a saddle point under PCM solvation. In the dimer minimum (**12D**), the two monomeric carbenoids are side-by-side, with one upside down relative to the other. This structure is the dimer of carbenoid **12**. In the planar transition state (**TS31**), one carbenoid is directly on top of the other, and also upside down. No structure corresponding to a dimer of linear carbenoids could be located.

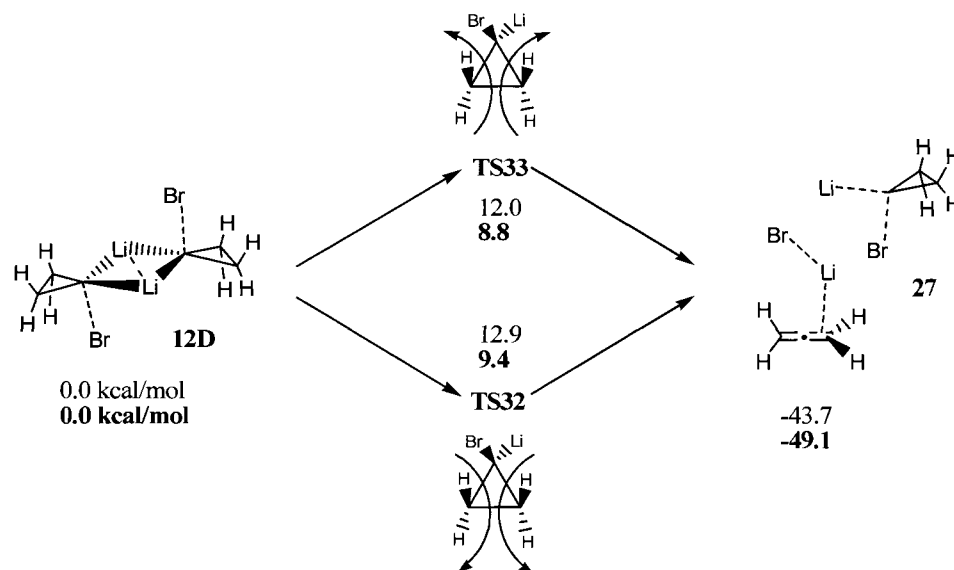
Scheme 2-12. B3LYP/6-31+G(d) and B3LYP/6-31+G(d) with PCM solvation in diethyl ether energies and free energies in kcal/mol for dimerization of bent carbenoid **12**.



ΔE (<i>in silico</i>)	-42.2	-36.6
ΔE (PCM)	-13.1	n/a
ΔG (<i>in silico</i>)	-30.5	-24.4
ΔG (PCM)	-1.3	n/a

According to B3LYP/6-31+G(d) calculations, dimerization is energetically favorable both *in silico* and in solution (Scheme 2-12). Ring opening of one carbenoid in the dimer was considered, holding the other constant. Like the monomers, the dimer has two transition states for ring opening (**TS32** and **TS33**, Scheme 2-13), corresponding to the two possible disrotatory modes. For the parent dimer, the lower energy transition state has the same mode of disrotatory ring opening as the parent monomer (**TS33**), where the hydrogens *syn* to bromine rotate outward.

Scheme 2-13. B3LYP/6-31+G(d) and B3LYP/6-311+G(d,p) energetics for ring opening of parent dimer **12D**.

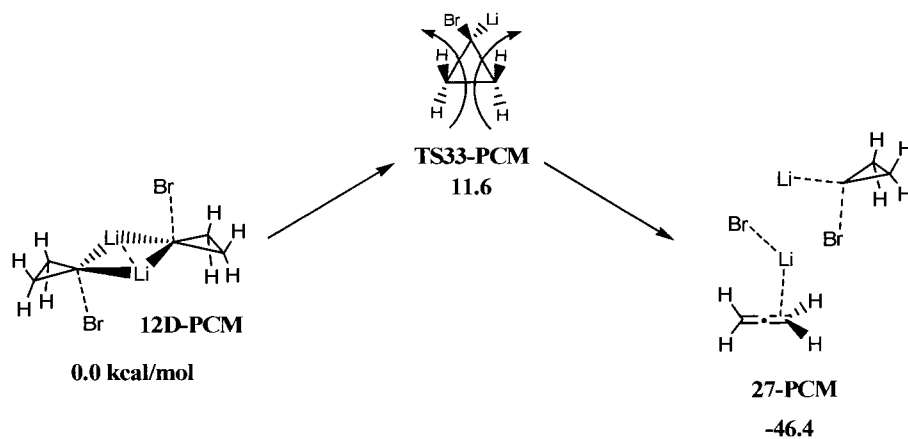


Ring opening proceeds exactly analogously to the monomers, with disrotatory and then conrotatory motion. The IRC calculation for the ring opening of **12D** through **TS33** repeatedly claims to have located a minimum long before the allene is formed. Attempts to optimize this structure as a minimum lead directly to the allene and a frequency analysis shows mode that has an imaginary frequency, which is physically meaningless. This structure is not a minimum, but expected to be the VRI point. Surface symmetry likely confuses the calculation of the gradient, as there would exist two vectors of equal magnitude in different directions. Without a unique gradient, the IRC calculation declares this point a minimum.

Implicit solvation models were also implemented for the parent dimers, with results akin to *in silico* calculations. The *in silico* calculations predict a dimer and a transition state for monomer exchange, but the PCM calculations show only the minimum (**12D-PCM**). The reaction barrier in solution is comparable to the gas phase barrier. Scheme 2-13 is reproduced as Scheme 2-14 with these results. The transition

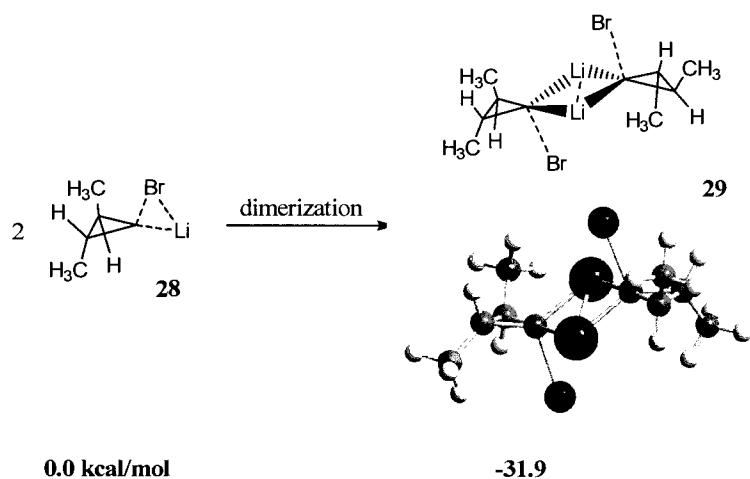
state with the hydrogens *syn* to bromine rotating inward failed to optimize (**TS32-PCM**). This may suggest that there is only one transition state for dimeric ring opening in solution.

Scheme 2-14. Implicit solvation for ring opening of dimer **12D-PCM** computed at B3LYP/6-31+G(d) with PCM solvation in diethyl ether



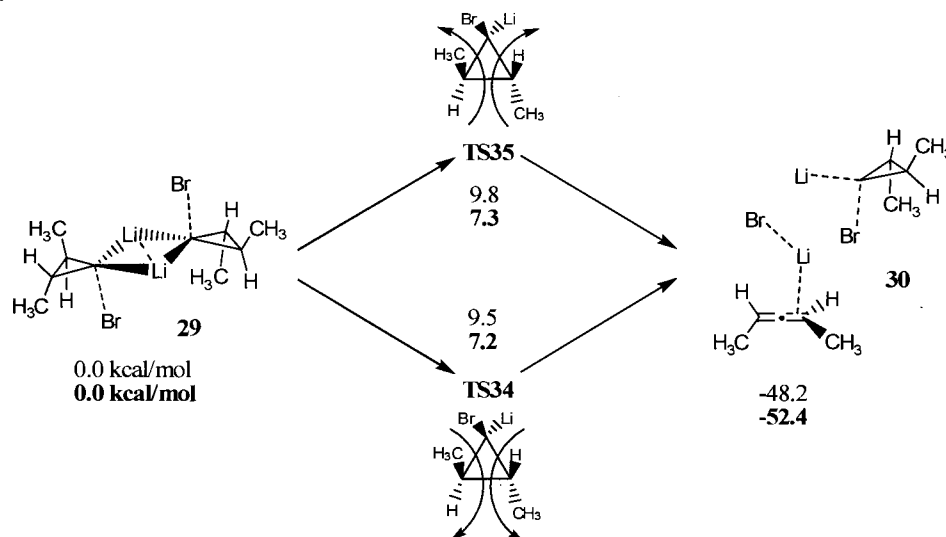
To confirm the stereochemical pathway traced by the chiral monomers, *trans* dimethyl dimers were constructed. Like the parent monomers, dimerization is energetically favorable, though there is only one dimer structure (**29**, Scheme 2-15). Optimizations of trial structures for the planar dimer (transition state) led back to the original side-by-side structure.

Scheme 2-15. B3LYP/6-311+G(d,p) energetics and geometries for dimerization of bent dimethyl carbenoid **28**.



Again, there are two transition states for initial disrotatory ring opening (**TS34** and **TS35**, Scheme 2-16). In contrast to the parent dimers, the lower energy transition state for the dimethyl dimer has the groups *syn* to bromine rotating inward (**TS34**). Both transition states are of comparable energy, likely because both faces of the cyclopropyl ring are sterically equivalent.

Scheme 2-16. B3LYP/6-31+G(d) and B3LYP/6-311+G(d,p) energetics for the ring opening of dimethyl dimer **29**.



The dimethyl dimers do trace the same stereochemistry as the parent *trans*-dimethyl carbenoid. Both transition states lead to the same enantiomer of the allene-carbenoid complex (**30**). Figures 2-11 and 2-12 show the forward IRCs for ring opening of **29** through **TS34** and **TS35**, respectively.

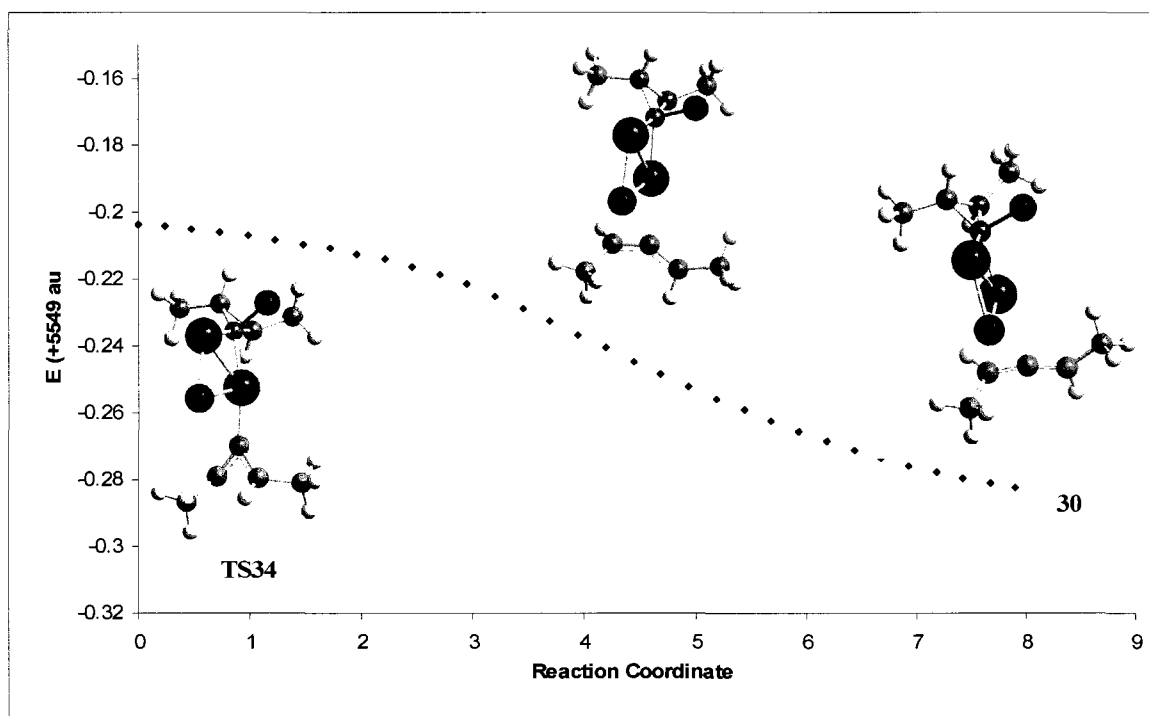


Figure 2-11. B3LYP/6-31+G(d) forward intrinsic reaction coordinate for ring opening of dimethyl dimer **29** through **TS34**.

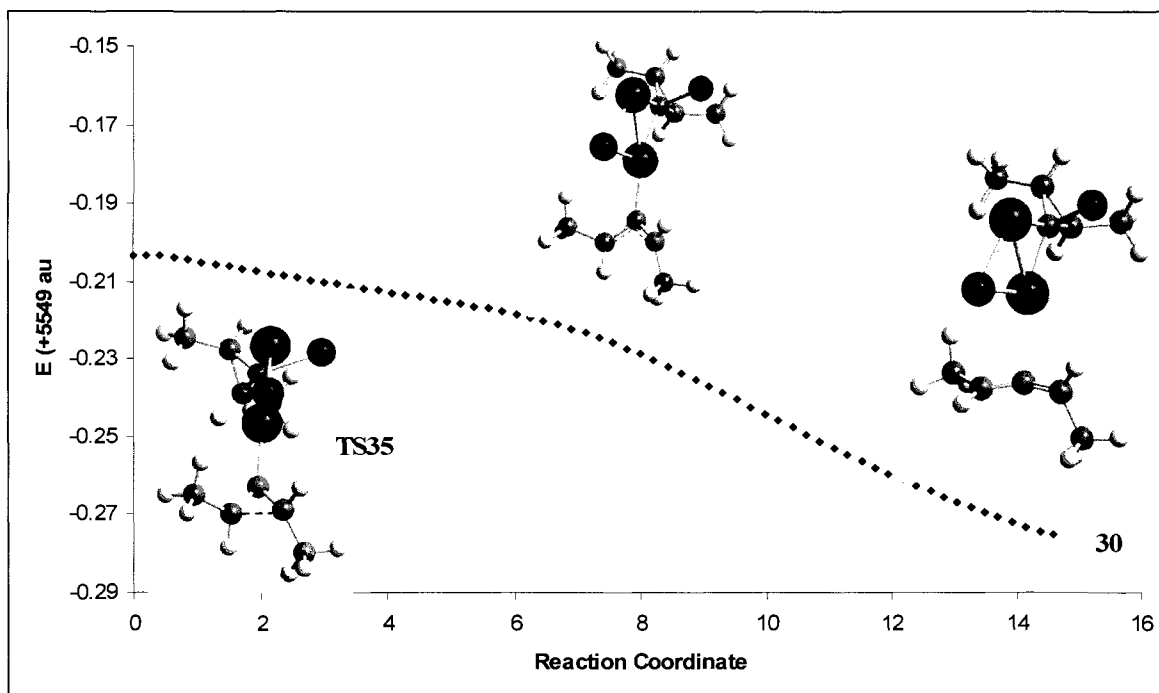


Figure 2-12. B3LYP/6-31+G(d) forward intrinsic reaction coordinate for ring opening of dimethyl dimer **29** through TS35.

^{13}C NMR predictions provide the most notable evidence that the monomer is not the species that participates in this reaction. For the *cis endo* bicyclic carbenoid (**23**), Seebach and coworkers showed that the carbenoid carbon has a ^{13}C chemical shift of 80.7 ppm relative to TMS.⁹⁴ B3LYP/6-311+G(2d,p) calculations, however, predict 201.7 ppm *in silico* and 213.1 ppm in diethyl ether. To address this discrepancy, dimer models of varying ring sizes were constructed and their corresponding ^{13}C NMR spectra were computed *in silico* and in diethyl ether. These chemical shifts were compared to the parent monomer and dimer, as well as the experimental results (Table 3). Here, C6 means a backbone structure of bicyclo[3.1.0]hexane, C7 means bicyclo[4.1.0]heptane, and C9 means bicyclo[6.1.0]nonane. All are *cis*-bicyclic structures and *endo/exo* refers to Br orientation relative to the longest bridge. It is clear that the dimer structures have chemical shifts that are in better agreement with experimental results, but they still differ

enough to warrant further work. It is also evident that solvation has only a minor effect on the predicted chemical shift.

Table 3. ^{13}C chemical shifts of the carbenoid carbon relative to TMS calculated at B3LYP/6-311+G(2d,p).

molecule	δ (ppm) <i>in silico</i>	δ (ppm) diethyl ether
parent monomer (12)	200.3	212.4
parent dimer (12D)	97.3	104.4
C6 <i>endo</i> monomer	221.6	233.9
C6 <i>exo</i> monomer	170.4	178.7
C6 dimer	119.1, 111.5	100.0, 104.0
C7 <i>endo</i> monomer	205.7	214.4
C7 <i>exo</i> monomer	170.4	180.2
C7 dimer	122.8, 119.2	128.9, 125.7
C9 <i>endo</i> monomer (23)	201.7	213.1
C9 <i>exo</i> monomer (24)	153.7	163.1
C9 dimer	117.8, 112.5	124.6, 118.9

Conclusions

Although the Doering-Moore-Skattebøl Rearrangement has been known for almost 50 years, the intricacies of its mechanism have not been characterized with high level computations. In the present work, the reaction mechanism, stereochemistry, effects of solvation, and reactions of dimeric carbenoids were modeled. For cyclopropyl LiBr carbenoids, there are two minima: one with linear C-Li-Br geometry, and another with triangular C-Li-Br geometry. Each can undergo disrotatory ring opening to an allene. Calculations with solvation, however, strongly favor a triangular carbenoid, which has carbanionic character. Even though *in silico* models predict that the one- and two-step ring opening processes are competitive, calculations with both implicit and explicit solvation show that single-step ring opening is the primary route. There are two transition states for direct ring opening of the triangular carbenoid. The hydrogens *syn* to

the bromine can rotate outward or inward. The outward transition state is lower in energy. Intrinsic reaction coordinate calculations show that ring opening is initially disrotatory and synchronous. After passage through a valley ridge inflection point, ring opening becomes conrotatory when one rotating group reverses direction.

Even though it has come to be synonymous with cyclopropylidene chemistry, this work predicts that free carbenes are actually not present in the reaction. Following lithium-halogen exchange, the rearrangement proceeds as a single step ring opening of a bent carbenoid to an allene, with lithium bromide dissociation occurring after the transition state is passed.

Ring opening of *cis* and *trans* bicyclic carbenoids offers efficient routes to cyclic allenes. For *cis* bicyclo[6.1.0]nonane carbenoids, there are two carbenoid diastereomers. The two diastereomers either have bromine *endo* or *exo* relative to the 6-carbon bridge. For each diastereomer, there are two ring opening transition states, corresponding to inward or outward rotation of the groups *syn* to bromine. The energetically favored transition state has the two ends of the 6-carbon bridge rotating away from each other. For the *endo* diastereomer, the 6-carbon bridge is *syn* to bromine; and for the *exo* diastereomer, the 6-carbon bridge is *anti* to bromine. Because both diastereomers are achiral, ring opening will produce a mixture of allene enantiomers.

Chiral *trans* bicyclic carbenoids open to a single allene enantiomer. In an important correlation with experiment, this carbenoid derived from (*R*)-*trans*-cyclooctene was shown to open to (*R*)-1,2-cyclononadiene, precisely as observed by Cope in 1970.⁶⁸ Stereochemical results can be correlated with a least motion pathway for ring opening. The hydrogens undergo most of the movement, while the 6-carbon bridge remains almost

in place. The two direct ring opening transition states are close in energy since the two faces of the cyclopropyl ring are sterically equivalent. Intrinsic reaction coordinate calculations show initially synchronous disrotatory ring opening that becomes asynchronous disrotatory when one group ceases rotating.

Carbenoid dimerization is predicted to be favorable in solution. There are two structures for carbenoid dimers: a minimum with the two individual carbenoids side-by-side, and a low energy transition state for the two monomers exchanging relative positions. Carbenoid dimers have two modes of initial disrotatory ring opening, where the groups *syn* to the bromine can rotate either inward or outward. For the parent dimers, the lower energy transition state has the hydrogens *syn* to bromine rotating outward. Calculations with PCM solvation do not significantly change the reaction energetics. Since the geometries and energetics of the dimer pathway match well their monomer counterparts, the monomers are appropriate models to describe the progression of the rearrangement. Though ^{13}C NMR predictions for the dimers are closer to experimental findings, they deviate enough to call for further work.

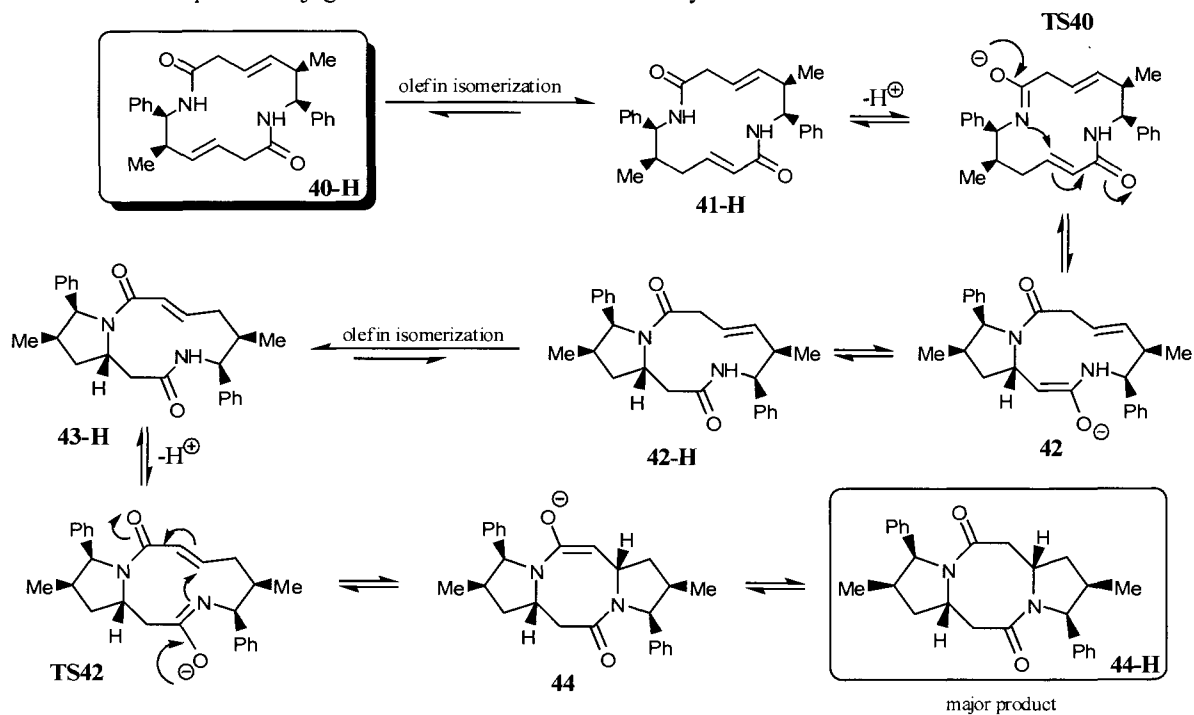
CHAPTER III

BIS-LACTAM CYCLIZATIONS

Introduction

Porco's group at Boston University recently studied a complex series of bis-lactam cyclizations.⁹⁵ In the presence of base, bis-lactam **40-H** twice undergoes transannular cyclization to give **44-H** as the major product, where **H** indicates the species is protonated. A proposed mechanism is outlined in Scheme 3-1. Conjugation must precede transannular cyclization. The mono-deprotonated lactam then undergoes a transannular cyclization (**TS40**) to form **42**, which is in equilibrium with its neutral counterpart (**42-H**). These steps then repeat, where the neutral monocyclized lactam isomerizes to **43-H**, is deprotonated, and closes transannularly (**TS41**) to give the bicyclized structure **44**. This product is also in equilibrium with its neutral counterpart **44-H**. The mechanism showing the experimentally observed stereochemistry is given in Scheme 3-1.

Scheme 3-1. Proposed conjugate addition mechanism for the cyclization of bis-lactam **40-H**.



The stereochemistry of each cyclization can follow one of two pathways according to the orientation of the hydrogen across the ring. This leads to three possible bicyclized diastereomers **44-H**, **45-H**, and **46-H**. Experimental results show one major product **44-H** in addition to minor diastereomers **45-H** and **46-H**. Structures for the starting material and three possible products are shown in Figure 3-1.

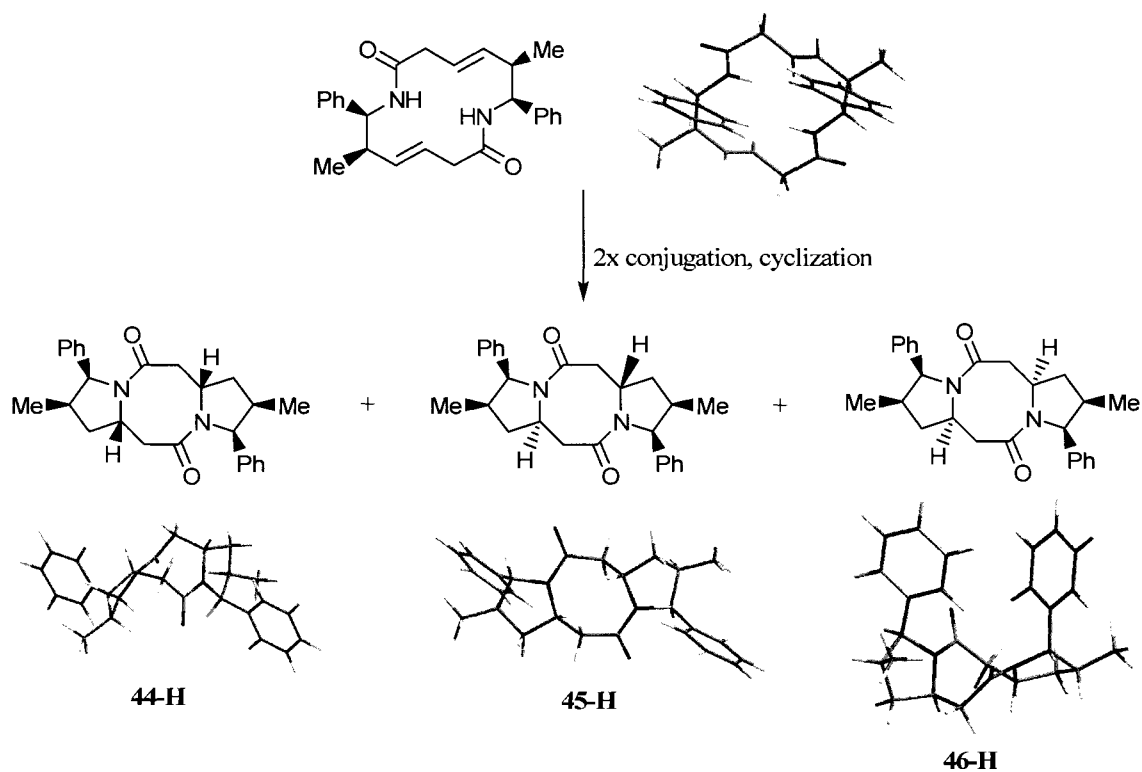


Figure 3-1. Summary and structures of major products from the cyclization of bis-lactam **40-H**.

To understand this distribution of products, computational studies were carried out based on the proposed mechanism. This proved to be a very challenging problem. The difficulty in studying macrocycles by computation is a consequence of their flexibility, yielding hundreds or thousands of conformations. This same complexity exists for transition state searching. There are very few examples of simultaneously and systematically searching both conformations and transition states.⁹⁶⁻¹⁰⁰

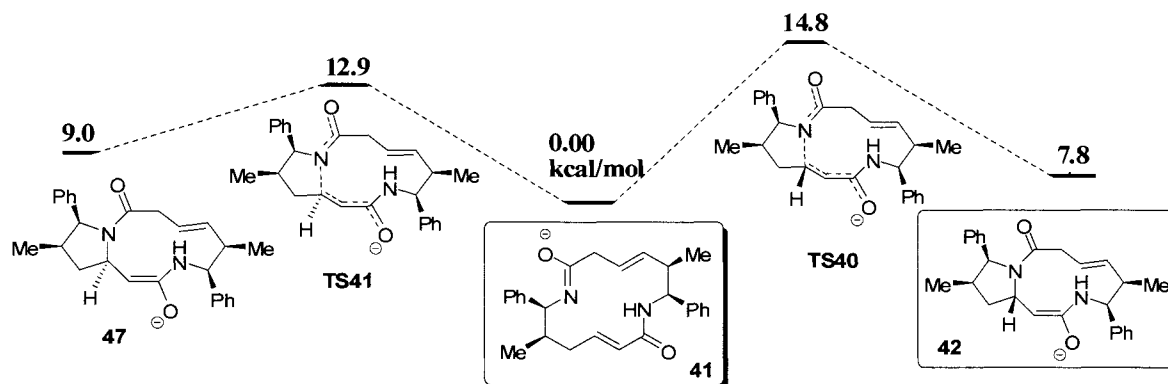
Results and Discussion

A computational method was developed to search conformations of stationary points on this surface. Given that these are such large molecules, it would be impractical to search 10,000 conformations at a high level of theory. For reference, a DFT optimization and frequency analysis on one of these structures takes approximately 3 days on a standard desktop PC or 24 hours on an 8 processor machine. As a compromise, low level conformation searches and geometry optimizations were initially done to establish the best structures for high level characterization. For each minimum, a set of candidate conformers was established by Monte Carlo methods using the Merck Molecular Force Field.¹¹⁰ Conformers were searched by rotation about each atom in the macrocycle, followed by energy minimization. The 50-100 structures of lowest energy were subjected to an AM1 geometry optimization followed by a single point HF/3-21G calculation. The lowest energy structure was optimized at the M05-2X/6-31G(d) level of theory. For transition states, a set of candidate conformers was established by Monte Carlo Methods using the Merck Molecular Force Field¹¹⁰ with a constrained distance of 1.9Å for the transannular bond. This is a typical bond distance for a ring closure transition state. Conformers were again searched by rotation about each atom in the macrocycle, followed by energy minimization. The 50-100 structures of lowest energy were subjected to an AM1 transition state optimization followed by a single point HF/3-21G calculation. The lowest energy structure was optimized as a first order saddle point at the M05-2X/6-31G(d) level of theory.

Conjugation and anionic transannular cyclization are slightly endothermic (Scheme 3-2), consistent with the Porco group's failure to isolate conjugated or anionic

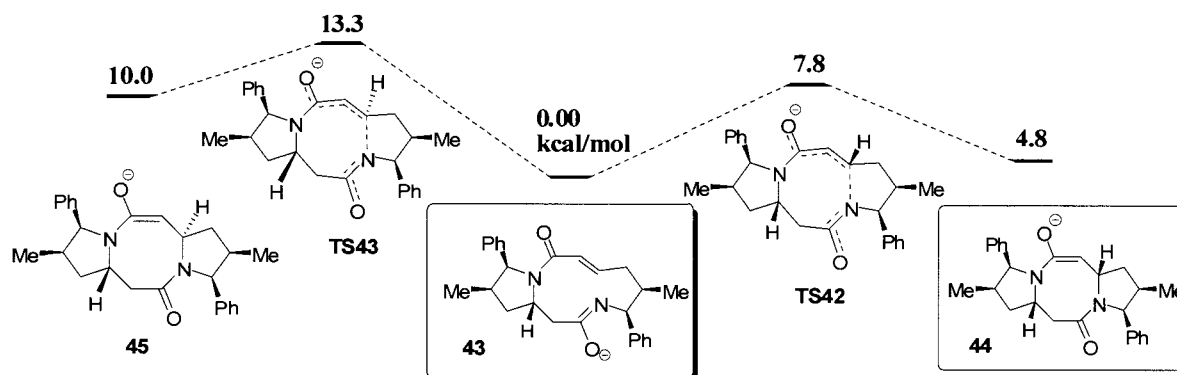
intermediates. For the neutral species, each conjugation costs approximately 2 kcal/mol. In the first anionic cyclization, there are two transition states for cyclization, one corresponding to each possible monocyclized diastereomer. Interestingly, the cyclization that leads to **47** has a lower barrier than the transition state leading to **42**. This would seem to suggest that the minor product pathway is favored over the major product pathway. However, since these cyclizations have modest barriers and are endothermic, under the given reaction conditions (60 °C, 24 hours), the product distribution must be thermodynamically controlled. Though the kinetically favored path would ultimately lead to a minor product (**47**), the thermodynamically favored path corresponds with experimentally observed stereochemistry (**TS40** to **42**).

Scheme 3-2. M05-2X/6-31G(d) energetics of the first anionic cyclization of bis-lactam **40-H**.



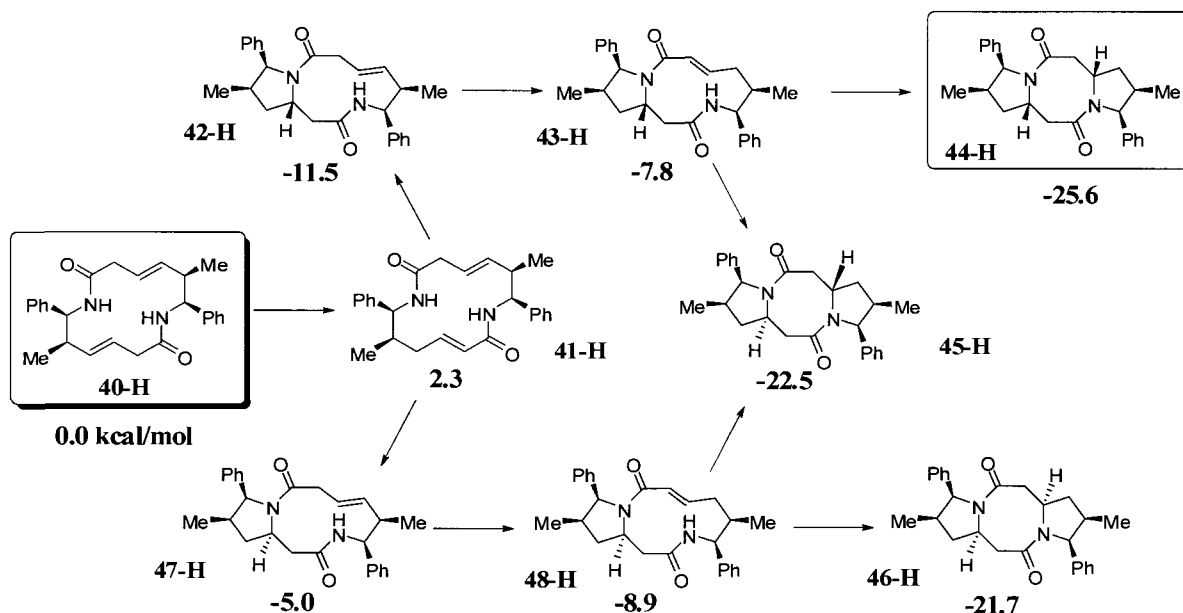
Assuming the first cyclization leads to the thermodynamically stable product (**42**), the second cyclization also has two possible pathways (**TS43** to **45** or **TS42** to **44**, Scheme 3-3). But in this case, the pathway leading to the experimentally observed major product (**44**) is both kinetically and thermodynamically favored since the transition state (**TS42**) has a lower barrier and the product is of lower energy.

Scheme 3-3. M05-2X/6-31G(d) energetics of the second anionic cyclization of bis-lactam **40-H**.



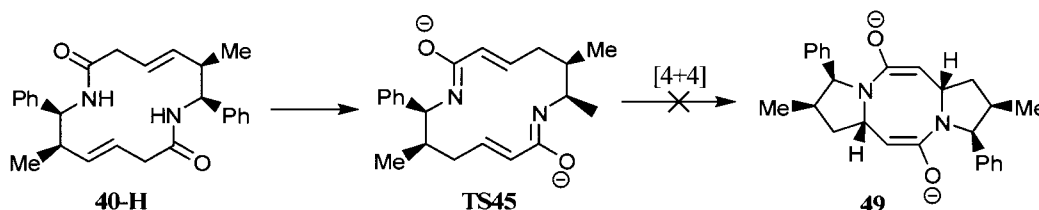
These anionic cyclizations are modestly endothermic, but upon reprotonation, the cyclization becomes substantially exothermic. The three neutral products are of comparable energy, with diastereomer **44-H** being lowest in energy, consistent with the experimental results showing **44-H** as the major product and **45-H** and **46-H** as minor products.

Scheme 3-4. M05-2X/6-31G(d) energetics for the neutral minima in the cyclization of bis-lactam **40-H**.



The possibility of a concerted [4+4] cycloaddition (**TS45**) was also examined (Scheme 3-5), but found to be substantially disfavored. The reaction is endothermic by 22 kcal/mol with a high barrier of 36 kcal/mol. In comparison with the two-step cyclization, the barrier is too high for this process to be significant.

Scheme 3-5. Concerted [4+4] cycloaddition mechanism for the cyclization of bis-lactam **40-H**



Conclusions

The cyclization of bis-lactam **40-H** is a thermodynamically controlled process that leads to one major diastereomer **44-H**, and two minor diastereomers **45-H**, and **46-H**. Since the anionic cyclizations are rapid and reversible and the reactions are carried out overnight at high temperature, the thermodynamic product is favored over the kinetic product. Given this, the two-step anionic process is favored over the high-energy concerted [4+4] cycloaddition.

In the first anionic cyclization, the thermodynamically favored pathway has a slightly higher barrier than the kinetic pathway. In the second anionic cyclization, the kinetic and thermodynamic pathways are the same, and this cyclization is consequently faster than the first. Though the anionic cyclizations are slightly endothermic, the neutral cyclizations, the protonated versions of their anionic counterparts, are substantially endothermic. The relative energies of these products agree with the experimentally observed product distribution.

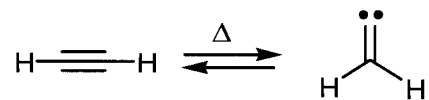
CHAPTER IV

THERMAL REARRANGEMENTS OF ORTHO-ETHYNYLTOLUENE

Introduction

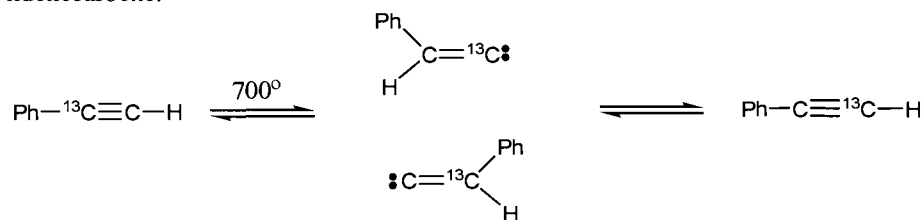
Alkynes are known to thermally interconvert with carbenes via the Brown rearrangement, a [1,2] hydrogen migration of an alkynyl hydrogen or other group (Scheme 4-1).

Scheme 4-1. The Brown Rearrangement



Brown first proposed this equilibration in 1974, when he pyrolyzed ^{13}C -labeled phenylacetylene and found that the label had scrambled. He explained these results by suggesting that at high temperature, phenylacetylene is in equilibrium with benzylicidene carbene (Scheme 4-2).¹⁰¹ He later elaborated upon this in a review.¹⁰²

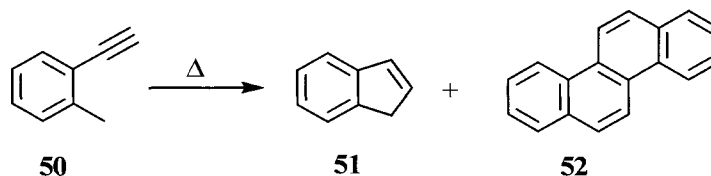
Scheme 4-2. Isotopic scrambling seen by Brown in 1974, suggesting phenylacetylene is in equilibrium with benzylicidene carbene.



In the flash vacuum pyrolysis of ortho-ethynltoluene reported in 1974, Brown obtained mostly indene and just 1% chrysene.¹⁰¹ He concluded that chrysene must be formed by a minor pathway. By graphite-sensitized microwave flash pyrolysis, however, Aida Ajaz has seen 47% conversion to indene and 28% conversion to chrysene.¹⁰³ This

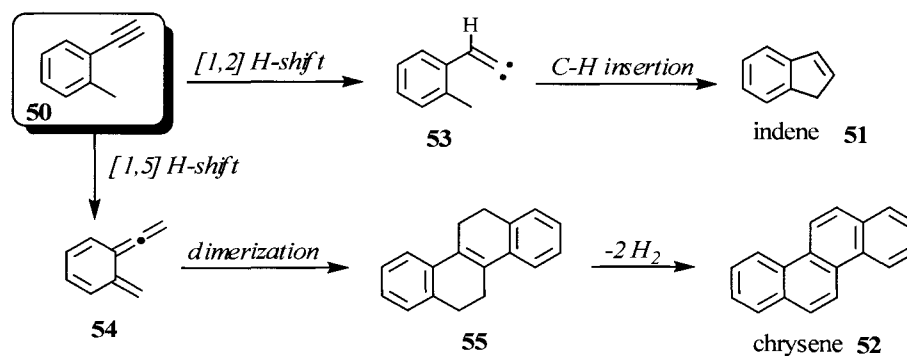
much higher yield of chrysene prompted computational exploration of possible pathways in this reaction. Brown's proposed mechanism is summarized in Scheme 4-4.

Scheme 4-3. Summary of the products from the pyrolysis of *o*-ethynyltoluene.



Upon heating, *o*-ethynyltoluene rearranges to indene, presumably through a Brown rearrangement (a [1,2] H-shift) followed by C-H insertion. A competitive [1,5] hydrogen migration is also possible, leading to the reactive intermediate **54**, termed here *ortho*-xylallene as an analogue of the well-known intermediate *ortho*-xylyene. Dimerization of *o*-xylallene followed by aromatization leads to chrysene. Brown speculated about a radical dimerization route to chrysene.¹⁰¹

Scheme 4-4. Summary of the competitive processes in the thermal rearrangement of *o*-ethynyltoluene to yield indene and chrysene.

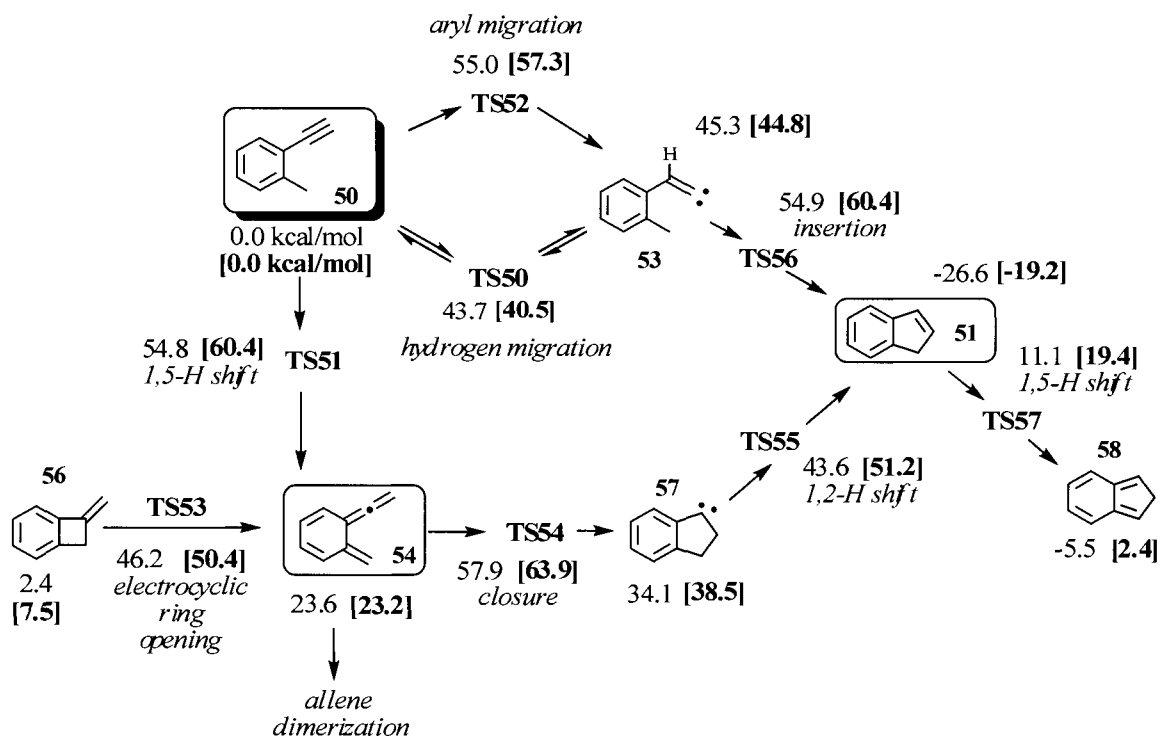


Results and Discussion

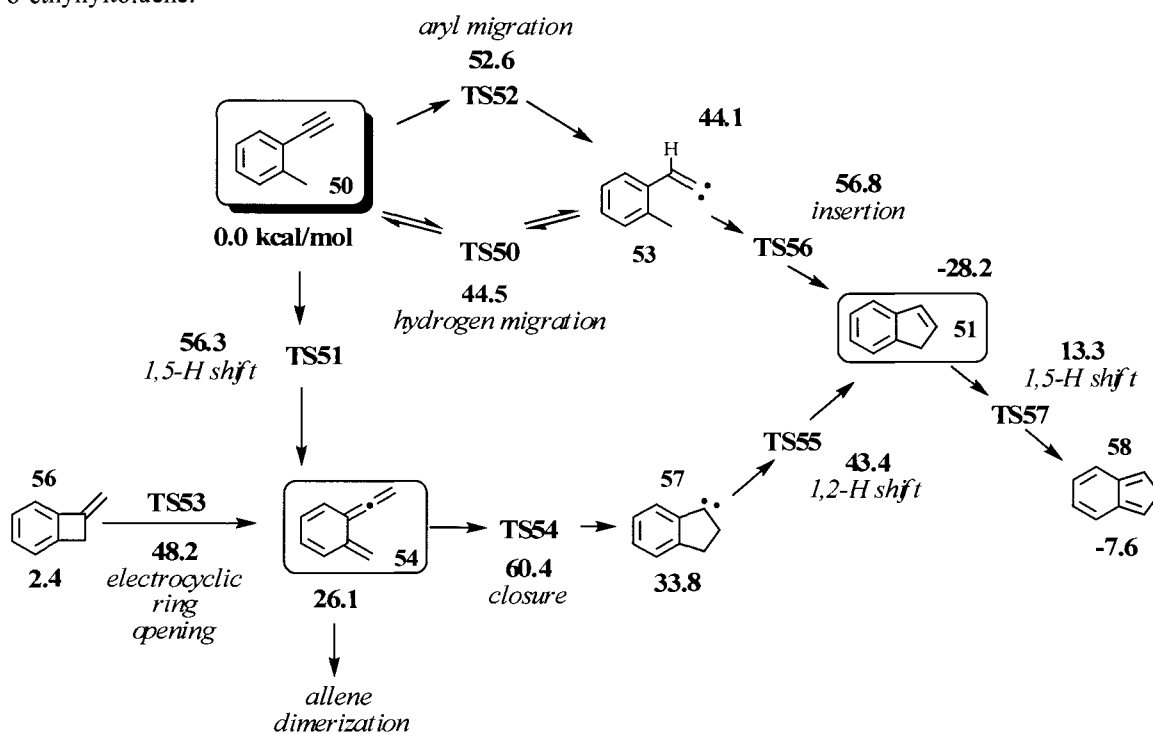
This reaction was studied with the well calibrated B3LYP density functional method¹⁰⁸ (Scheme 4-5). The initial [1,2] and the [1,5] shifts (**TS50** and **TS51**, respectively) are not competitive since their barriers differ by almost 10 kcal/mol. The [1,2] shift transition state (**TS50**) and the resulting carbene (**53**) are nearly isoenergetic, also consistent with a reversible hydrogen migration. An aryl migration is also possible (**TS52**) and would yield the same carbene, but its energy is high enough above the hydrogen migration to render it insignificant. Since the [1,2] migration is rapid and reversible, the rate-determining step is the C-H insertion (**TS56**) that occurs after the [1,2] shift. This insertion competes with the [1,5] shift (**TS51**), both of which have comparable barriers of approximately 55 kcal/mol. Note parenthetically that indene (**51**) is also in equilibrium with the slightly higher energy isoindene (**58**) through a [1,5] H-shift (**TS57**). Another possible route to o-xylallene is the electrocyclic ring opening of **56**. This was observed by Brown,¹⁰¹ who observed indene and ortho-ethynyltoluene as products in the pyrolysis of **56**. High temperature free energies (boldface, Scheme 4-5) were also computed to better account for experimental reaction conditions. By this comparison, C-H insertion and the [1,5] H-shift are nearly identical, further underscoring their competition.

To further support DFT results, CCSD(T) energies were computed at DFT geometries. Scheme 4-5 is reproduced as Scheme 4-6 with these results. Due to computer memory limitations, the smaller 6-311G(d) basis set was used. All CCSD(T) energies include DFT ZPVE corrections.

Scheme 4-5. B3LYP/6-311+G(d,p) energies and free energies at 898 K for the thermal rearrangements of o-ethynyltoluene (**50**) to indene (**51**) and the reactive intermediate ortho-xylallene (**54**).



Scheme 4-6. CCSD(T)/6-311G(d)//B3LYP/6-311+G(d,p) energetics for the thermal rearrangement of o-ethynyltoluene.



This overall CCSD(T) energy profile is remarkably similar to the DFT profile, as would be expected for closed shell hydrocarbons. Figure 4-1 shows the DFT geometries and the relative CCSD(T) energies.

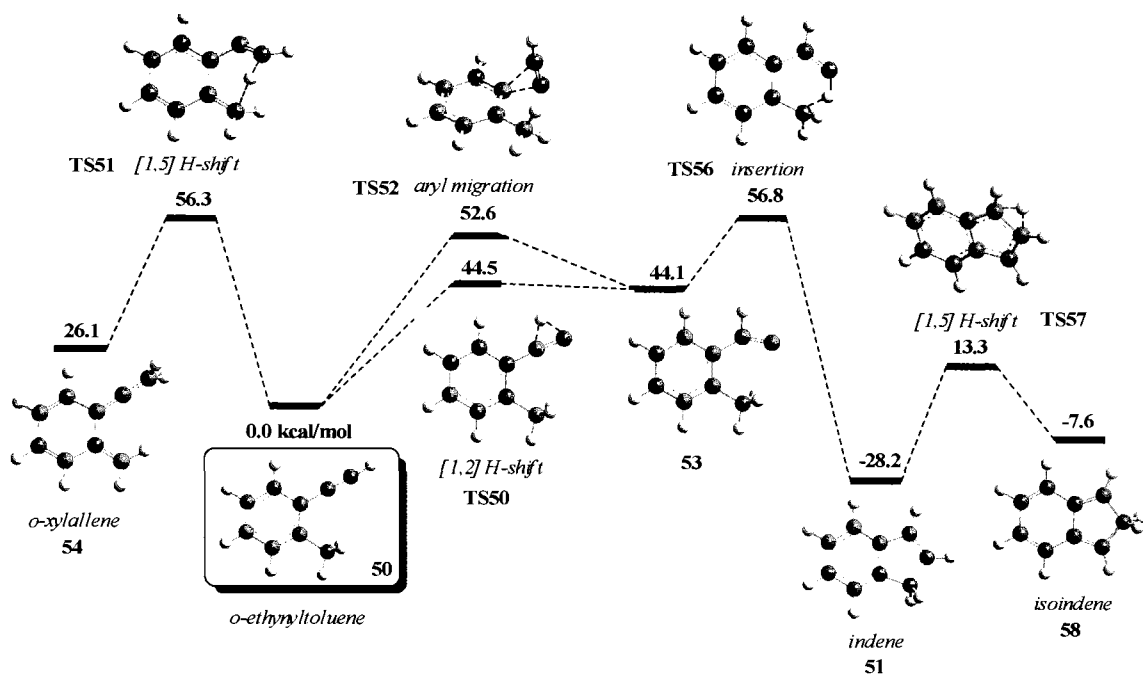


Figure 4-1. CCSD(T)/6-311G(d)//B3LYP/6-311+G(d,p) energetics and B3LYP/6-311+G(d,p) geometries for the thermal rearrangement of o-ethynyltoluene (50) to o-xylallene (54) and indene (51).

Dimerization of o-xylallene initiates the formation of chrysene. This dimerization (TS58) is analogous to that of traditional allenes, forming a bisallyl diradical (59) that closes in two steps (TS59 and TS60) to 61. Dehydrogenation can then yield chrysene. The first closure gives a structure with no open shell character ($S^2 = 0$). The second closure, therefore, is a simple intramolecular electrocyclization.

Scheme 4-7. Dimerization of ortho-xylallene (54).

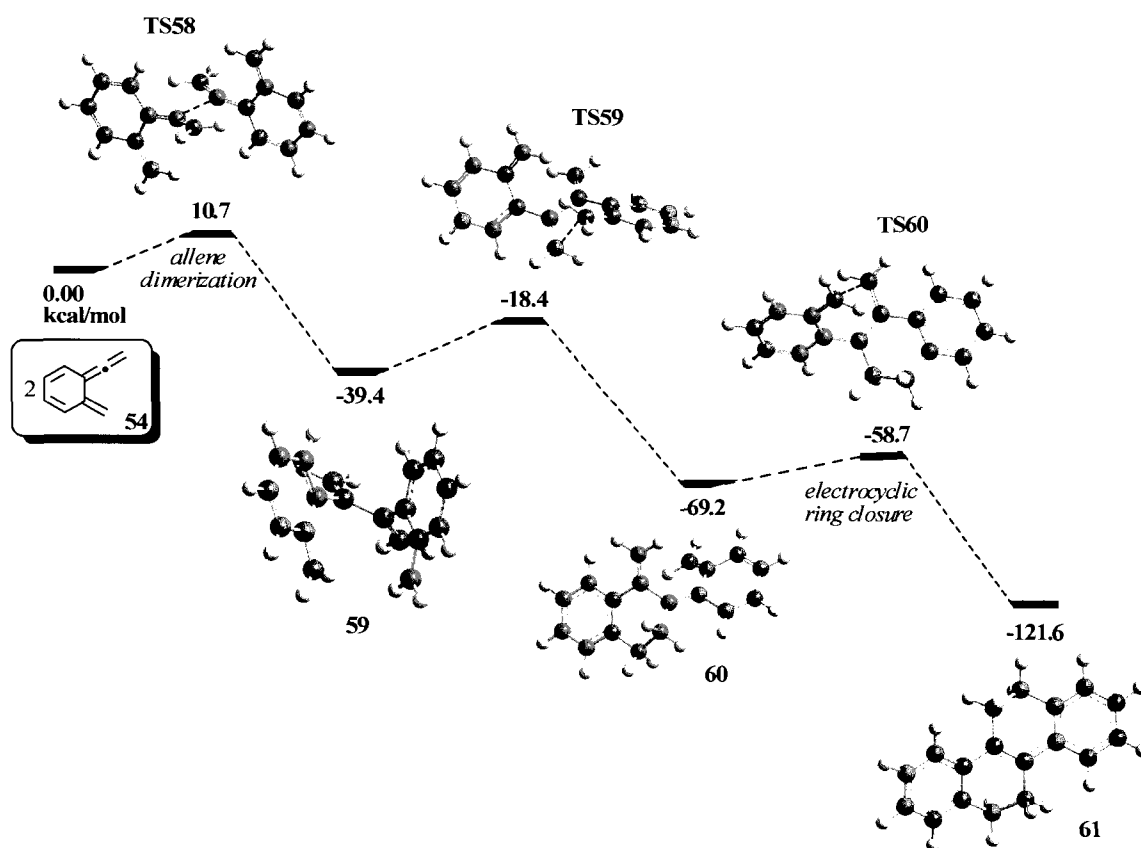
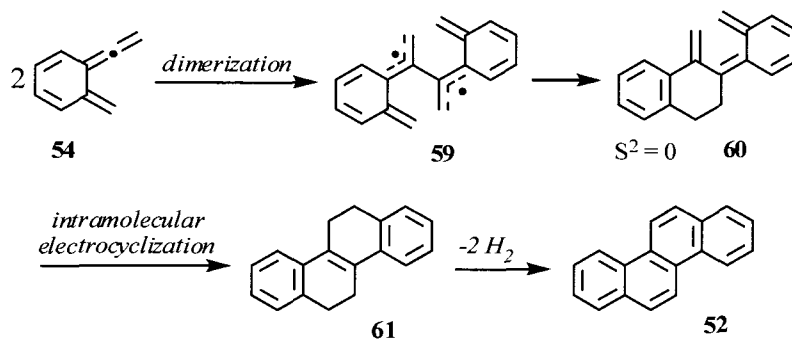
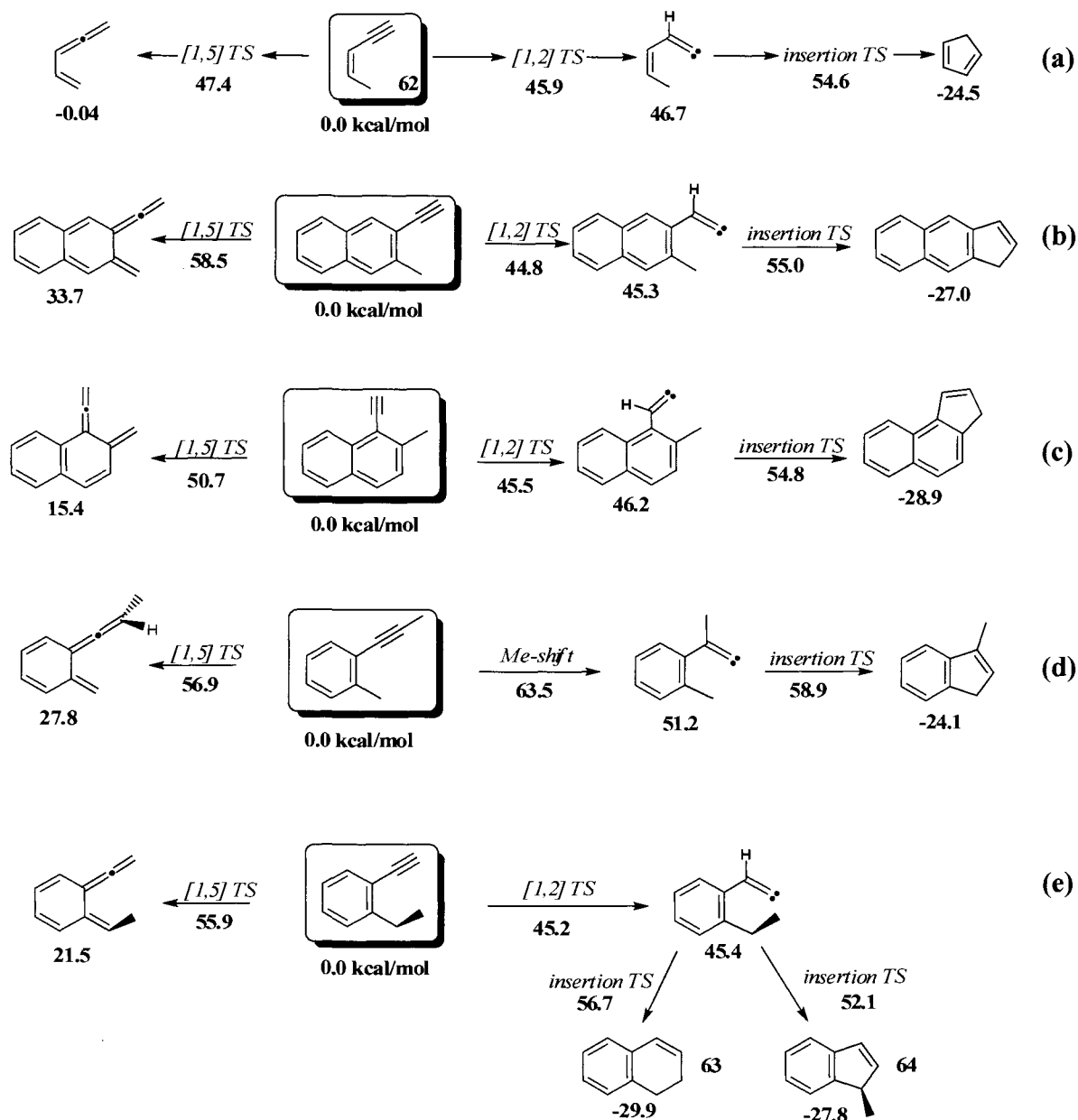


Figure 4-2. B3LYP/6-311+G(d,p) energetics and geometries for the dimerization of ortho-xylallene (54).

There is also a high energy pathway from o-xylallene (**54**) to indene (**51**), but dimerization has a more favorable barrier and is presumably driven by its substantial exothermicity. In this pathway, o-xylallene can close upon itself by **TS54** to form carbene **54**. Then a [1,2] H-shift will yield indene (Scheme 4-5). These processes are hardly competitive, though, since dimerization by **TS58** has a barrier of only 10.3 kcal/mol and closure by **TS54** has a much higher barrier of 34.3 kcal/mol. Dimerization occurs rapidly, rendering the closure noncompetitive.

One long-term goal of this work is to design initial structures such that the [1,5] pathway predominates, facilitating the synthesis of higher polyacenes. Scheme 4-8 summarizes these efforts. Since the rate-determining step along the [1,2] pathway is the C-H insertion, the comparisons to be made are the barriers to this insertion and the [1,5] H-shift.

Scheme 4-8. Comparisons of the B3LYP/6-311+G(d,p) energies for the [1,5] versus the C-H insertion transition states for structural variations of the ene-yne **62**.



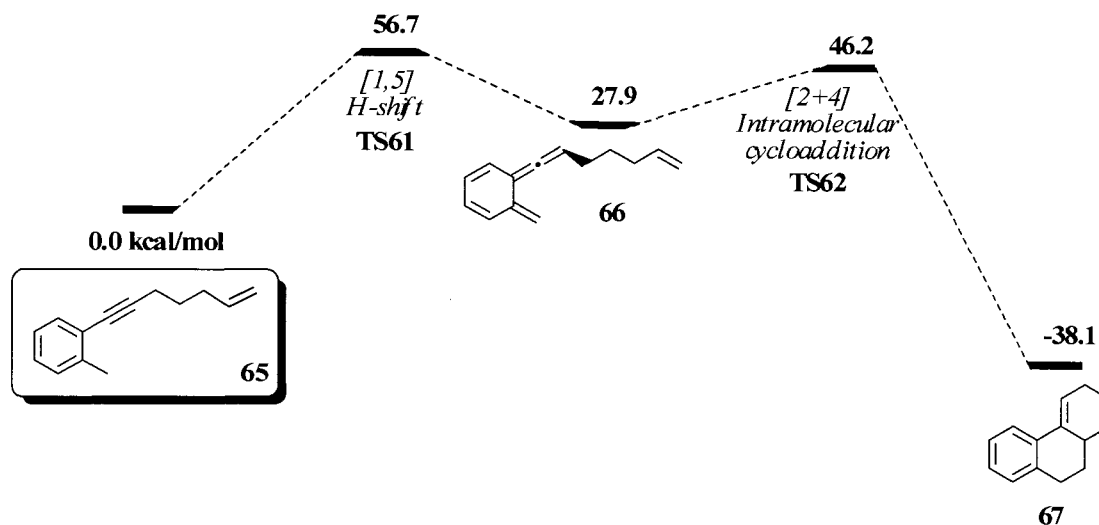
For reaction (c) the [1,5] shift has become increasingly favorable because of diminished loss of aromaticity, whereas the barrier to C-H insertion remains essentially unchanged. By contrast in (b), the [1,5] shift breaks aromaticity in both rings and the

barrier increases. Not surprisingly with its lack of aromaticity, the parent rearrangement **(a)** produces a nearly isoenergetic allene through a [1,5] H-shift.

Replacing the alkynyl hydrogen with a methyl group **(d)** is also an attractive alternative for tipping the reaction in favor of the [1,5] shift. The barrier to the methyl shift is much higher in energy than the facile hydrogen shift, as is typical, and the insertion transition state is correspondingly higher in energy. If *o*-ethynyltoluene is replaced with 1-ethyl-2-ethynylbenzene **(e)** (i.e. swapping the methyl group for an ethyl group), the [1,5] pathway is slightly stabilized. Along the vinylidene pathway, there are two possible C-H insertions. They are of comparable energy, but formation of methyl-substituted indene **64** is slightly more favorable than **63**. Each of these cases awaits experimental study.

Other possible applications include using this chemistry to study intramolecular *o*-xylallene cycloadditions to yield higher polycyclic compounds. For example, the [1,5] shift of **65** (TS61) leads to allene **66**, and an intramolecular Diels-Alder reaction (TS62) leads to **67**. Computations suggest favorable energetics for this route (Scheme 4-9).

Scheme 4-9. Potential application of the chemistry of *o*-xylallene calculated at B3LYP/6-311+G(d,p).



Conclusions

In 1974, Brown and coworkers showed that flash vacuum pyrolysis of ortho-ethynyltoluene yields indene and chrysene, the products of competitive pathways initiated by either a [1,5] or a [1,2] hydrogen migration.^{101, 102} Indene is formed by a Brown rearrangement followed by C-H insertion. Chrysene is formed by a [1,5] hydrogen migration to the intermediate ortho-xylallene, which dimerizes, closes, and loses H₂. Aida Ajaz has found that microwave flash pyrolysis greatly increases the yield of chrysene,¹⁰³ presumably due to a high transient concentration of o-xylallene. This dimerization is similar to allene dimerization yielding a bisallyl diradical that closes in two steps.

The rate of formation of indene is determined by the C-H insertion that occurs after the reversible [1,2] H-shift. So the product distribution is determined by the relative energies of the [1,5] hydrogen migration and the C-H insertion. Computations on structural variations of o-ethynyltoluene show that competition between the [1,2] and the [1,5] hydrogen migrations should be dependent on structure, but these predictions need to be verified by experiment.

LIST OF REFERENCES

1. Harries, C., On oxidations by means of ozone. [machine translation]. *Ber. Deut. Chem. Ges.* **1903**, *36*, 1933-36.
2. Harries, C., Action of ozone on organic compounds. 1. *Liebigs. Ann. Chem.* **1905**, *343*, 311-74.
3. Harries, C., Action of Ozone on Organic Compounds. II. *Liebigs. Ann. Chem.* **1910**, *374*, 288-368.
4. Briner, E.; Demolis, A.; Paillard, H., The ozonization of aldehydes. The action of ozone and the participation of oxygen in the reaction. *Helv. Chim. Acta* **1931**, *14*, 794-803.
5. Fischer, F. G.; Dull, H.; Volz, J. L., Action of ozone upon aldehydes. *Liebigs. Ann. Chem.* **1931**, *486*, 80-94.
6. Briner, E.; Biedermann, H., Investigation of the role of ozone as catalyst of oxidation. III. Peculiarities of the chemical reactivity of ozone in the absence of oxygen, in the cases of the ozonization of benzaldehyde and sodium sulfite. *Helv. Chim. Acta* **1932**, *15*, 1227-34.
7. Briner, E.; Demolis, A.; Paillard, H., Ozone as a catalyst of oxidation; ozonization of benzaldehyde. *J. Chim. Phys. Phys.-Chim. Biol.* **1932**, *29*, 339-61.
8. Briner, E.; Demolis, A.; Paillard, H., Ozonization of benzaldehyde and the role of ozone as a catalyst of oxidation. II. *Helv. Chim. Acta* **1932**, *15*, 201-13.
9. Briner, E.; Lardon, A., Ozone as an oxidation catalyst. XI. Ozonization of aliphatic aldehydes in various solvents and in the gaseous state. *Helv. Chim. Acta* **1936**, *19*, 850-7.
10. Briner, E.; Lardon, A., Ozone as an oxidation catalyst. XIII. Rate of change of systems obtained by the ozonization of aldehydes. *Helv. Chim. Acta* **1936**, *19*, 1062-74.
11. Spath, E.; Pailer, M.; Gergely, G., Formation of phenols in the ozonization of benzene derivatives. II. Ozonization of methoxy-substituted aldehydes and the corresponding cinnamic acid esters. *Berichte der Deutschen Chemischen Gesellschaft [Abteilung] B: Abhandlungen* **1940**, *73B*, 795-804.
12. v. Wacek, A.; Eppinger, H. O., Peroxidative degradation of substituted aromatic aldehydes and ketones to the corresponding phenols. *Berichte der Deutschen Chemischen Gesellschaft [Abteilung] B: Abhandlungen* **1940**, *73B*, 644-51.
13. Briner, E.; Wenger, P., Oxidation of aldehydes catalyzed by ozone-effect of solvent, surface action and the presence of antioxidants. *Helv. Chim. Acta* **1943**, *26*, 30-8.
14. Briner, E., Accelerating action of ozone in the autoxidation processes. *Advances in Chemistry Series* **1959**, *No. 21*, 184-94.

15. Dick, C. R.; Hanna, R. F., Aromatic peracids. Effects of solvent on the ozone-initiated autoxidation of benzaldehydes. *J. Org. Chem.* **1964**, *29* (5), 1218-20.
16. Loan, L. D.; Murray, R. W.; Story, P. R., The mechanism of ozonolysis. Formation of cross ozonides. *J. Am. Chem. Soc.* **1965**, *87* (4), 737-41.
17. White, H. M.; Bailey, P. S., Ozonation of aromatic aldehydes. *J. Org. Chem.* **1965**, *30* (9), 3037-41.
18. Erickson, R. E.; Bakalik, D.; Richards, C.; Scanlon, M.; Huddlest.G, Mechanism of Ozonation Reactions .2. Aldehydes. *J. Org. Chem.* **1966**, *31* (2), 461-&.
19. Syrov, A. A.; Tsyskovskii, V. K., Mechanism of the action of ozone on aldehydes. *Zh. Org. Khim.* **1970**, *6* (7), 1392-8.
20. Sary, F. E.; Emge, D. E.; Murray, R. W., Hydrotrioxides - Formation and Kinetics of Decomposition. *J. Am. Chem. Soc.* **1974**, *96* (17), 5671-2.
21. Sary, F. E.; Emge, D. E.; Murray, R. W., Ozonation of Organic Substrates - Hydrotrioxide Formation and Decomposition to Give Singlet Oxygen. *J. Am. Chem. Soc.* **1976**, *98* (7), 1880-4.
22. Galstyan, G. A.; Pluzhnik, I. M.; Galstyan, A. G.; Potapenko, E. V., The kinetics and mechanism of the reaction of ozone with benzaldehyde and its derivatives in acetic acid. *Kinet. Catal.* **1998**, *39* (5), 682-5.
23. Klopman, G.; Joiner, C. M., New evidence in the mechanism of ozonolysis of olefins. *J. Am. Chem. Soc.* **1975**, *97* (18), 5287-8.
24. Klopman, G.; Andreozzi, P., The mechanism of ozonolysis. II. *Bull. Soc. Chim. Belg.* **1977**, *86* (6), 481-5.
25. Martinez, R. I., The Mechanism of O₃-Aldehyde Reactions. *Int. J. Chem. Kinet.* **1982**, *14* (3), 237-49.
26. Giamalva, D. H.; Church, D. F.; Pryor, W. A., Kinetics of Ozonation .5. Reactions of Ozone with Carbon-Hydrogen Bonds. *J. Am. Chem. Soc.* **1986**, *108* (24), 7678-81.
27. Yang, J.; Li, Q. S.; Zhang, S., Direct dynamics study on the reaction of acetaldehyde with ozone. *J. Comput. Chem.* **2007**, *29* (2), 247-55.
28. Cerkovnik, J.; Plesnicar, B.; Koller, J.; Tuttle, T., Hydrotrioxides Rather than Cyclic Tetraoxides (Tetraoxolanes) as the Primary Reaction Intermediates in the Low-Temperature Ozonation of Aldehydes. The Case of Benzaldehyde. *J. Org. Chem.* **2009**, *74* (1), 96-101.
29. Konrad, K. M., Master of Science Thesis, University of New Hampshire. **2006**.

30. Hoigne, J.; Bader, H., Ozonation of water. Role of hydroxyl radicals as oxidizing intermediates. *Science (Washington, DC, U. S.)* **1975**, *190* (4216), 782-4.
31. Hoigne, J.; Bader, H., The role of hydroxyl radical reactions in ozonation processes in aqueous solutions. *Water Res.* **1976**, *10* (5), 377-86.
32. Taube, H.; Bray, W. C., Chain reactions in aqueous solutions containing ozone, hydrogen peroxide and acid. *J. Am. Chem. Soc.* **1940**, *62*, 3357-73.
33. Chalmet, S.; Ruiz-Lopez Manuel, F., The structures of ozone and HOx radicals in aqueous solution from combined quantum/classical molecular dynamics simulations. *The J. Chem. Phys.* **2006**, *124* (19), 194502.
34. Weiss, J., The radical HO₂ in solution. *Transactions of the Faraday Society* **1935**, *31*, 668-81.
35. Lin, J.; Nakajima, T., An AM1 study of decomposition of aqueous ozone. *Theochem* **2003**, *625*, 161-7.
36. Koller, J.; Plesnicar, B., Mechanism of the Participation of Water in the Decomposition of Hydrogen Trioxide (HOOOH). A Theoretical Study. *J. Am. Chem. Soc.* **1996**, *118* (10), 2470-2.
37. Munoz, F.; Mvula, E.; Braslavsky, S. E.; von Sonntag, C., Singlet dioxygen formation in ozone reactions in aqueous solution. *J. Chem. Soc., Perkin Trans. 2* **2001**, (7), 1109-16.
38. Fabian, I., Reactive intermediates in aqueous ozone decomposition: a mechanistic approach. *Pure Appl. Chem.* **2006**, *78* (8), 1559-70.
39. Abel, E., The self-decomposition of ozone in aqueous solution. *Monatsh. Chem.* **1955**, *86*, 44-51.
40. Peleg, M., The chemistry of ozone in the treatment of water. *Water Res.* **1976**, *10* (5), 361-5.
41. Hausler, R.; Beron, P.; Briere, F., Ozonation mechanisms in water treatment. *Sciences et Techniques de l'Eau* **1990**, *23* (4), 351-64.
42. Hoigne, J., Chemistry of aqueous ozone and transformation of pollutants by ozonation and advanced oxidation processes. *Handbook of Environmental Chemistry* **1998**, *5* (Pt. C), 83-141.
43. Holcman, J.; Domaradzki, M., Fundamental reactions of ozone in the water environment. *Ekologia i Technika* **2003**, *11* (2), 16-9.
44. Wojtowicz, J. A., Ozone. *Kirk-Othmer Encyclopedia of Chemical Technology (5th Edition)* **2006**, *17*, 768-822.

45. Rothmund, V.; Burgstaller, A., Velocity of Decomposition of Ozone in Aqueous Solution. *Monatsh. Chem.* **1913**, *34*, 665-92.
46. Stumm, W., The decomposition of ozone in water solution. *Helv. Chim. Acta* **1954**, *37*, 773-8.
47. Kilpatrick, M. L.; Herrick, C. C.; Kilpatrick, M., The decomposition of ozone in aqueous solution. *J. Am. Chem. Soc.* **1956**, *78*, 1784-9.
48. Hewes, C. G.; Davison, R. R., Kinetics of ozone decomposition and reaction with organics in water. *AIChE J.* **1971**, *17* (1), 141-7.
49. Gurol, M. D.; Singer, P. C., Kinetics of ozone decomposition: a dynamic approach. *Environ. Sci. Technol.* **1982**, *16* (7), 377-83.
50. Tomiyasu, H.; Fukutomi, H.; Gordon, G., Kinetics and mechanism of ozone decomposition in basic aqueous solution. *Inorg. Chem.* **1985**, *24* (19), 2962-6.
51. Chelkowska, K.; Grasso, D.; Fabian, I.; Gordon, G., Numerical simulations of aqueous ozone decomposition. *Ozone: Sci. Eng.* **1992**, *14* (1), 33-49.
52. Sotelo, J. L.; Beltran, F. J.; Benitez, F. J.; Beltran-Heredia, J., Ozone decomposition in water: kinetic study. *Ind. Eng. Chem. Res.* **1987**, *26* (1), 39-43.
53. Kuosa, M.; Haario, H.; Kallas, J., Axial Dispersion Model for Estimation of Ozone Self-Decomposition. *Ozone: Sci. Eng.* **2005**, *27* (5), 409-17.
54. Ershov, B. G.; Morozov, P. A., Decomposition of ozone in water at pH 4-8. *Russ. J. Appl. Chem.* **2008**, *81* (11), 1895-8.
55. Lovato, M. E.; Martin, C. A.; Cassano, A. E., A reaction kinetic model for ozone decomposition in aqueous media valid for neutral and acidic pH. *Chem. Eng. J. (Amsterdam, Neth.)* **2009**, *146* (3), 486-97.
56. Braslavsky, S.; Heicklen, J., The gas-phase reaction of ozone with formaldehyde. *Int. J. Chem. Kinet.* **1976**, *8* (6), 801-8.
57. Pshezhetskii, S. Y., Morozov, N.M., Kamensetskaya, S.A., Siryatskaya, V.N., Gribova, E.I., Kinetics of the thermal decomposition of ozone. *Russ. J. Phys. Chem.* **1959**, *33*.
58. Glissmann, A., Schumacher, H.J., Der thermische Ozonzerfall. *Z. Phys. Chem. Abt. B.* **1933**, *21*, 323-48.
59. Voukides, A. C.; Konrad, K. M.; Johnson, R. P., Competing Mechanistic Channels in the Oxidation of Aldehydes by Ozone. *J. Org. Chem.* **2009**, *74* (5), 2108-13.

60. v. E. Doering, W.; LaFlamme, P. M., A two-step synthesis of Allenes from olefins. *Tetrahedron* **1958**, *2*, 75-9.
61. Moore, W. R.; Ward, H. R., Reactions of gem-dibromocyclopropanes with alkyllithium reagents. Formation of allenes, spiropentanes, and a derivative of bicyclopropylidene. *J. Org. Chem.* **1960**, *25*, 2073.
62. Moore, W. R.; Ward, H. R.; Merritt, R. F., The formation of highly strained systems by the intra-molecular insertion of a cyclopropylidene: tricyclo-[4.1.0.02,7] heptane and tricyclo [4.1.0.03,7] heptane. *J. Am. Chem. Soc.* **1961**, *83*, 2019-20.
63. Moore, W. R.; Ward, H. R., Formation of allenes from gem-dihalocyclopropanes by reaction with alkyllithium reagents. *J. Org. Chem.* **1962**, *27*, 4179-81.
64. Skattebol, L., Allenes from gem-dihalocyclopropane derivatives and alkyllithium. *Tetrahedron Lett.* **1961**, 167-72.
65. Skatteboel, L., Reactions of some 1,1-dibromo-2-alkenylcyclopropanes with methylithium. Intramolecular addition of a carbene to a double bond. *Chem. Ind. (London, U. K.)* **1962**, 2146-7.
66. Skatteboel, L., Synthesis of allenes from 1,1-dihalocyclopropane derivatives and alkyllithium. *Acta Chem. Scand.* **1963**, *17* (6), 1683-93.
67. Skatteboel, L., Chemistry of gem-dihalocyclopropanes. V. Formation of tricyclo[4.1.0.04.6]heptane and derivatives. *J. Org. Chem.* **1966**, *31* (9), 2789-94.
68. Cope, A. C.; Moore, W. R.; Bach, R. D.; Winkler, H. J. S., Molecular asymmetry. IX. Partial resolution and asymmetric synthesis of 1,2-cyclononadiene. *J. Am. Chem. Soc.* **1970**, *92* (5), 1243-7.
69. Closs, G. L.; Moss, R. A., Carbenoid formation of arylcyclopropanes from olefins, benzal bromites, and organolithium compounds and from photolysis of aryldiazomethanes. *J. Am. Chem. Soc.* **1964**, *86* (19), 4042-53.
70. Clark, T.; Schleyer, P. v. R., The structures of the carbenoid CH₂FLi: ab initio MO calculations. *J. Chem. Soc., Chem. Commun.* **1979**, (20), 883-4.
71. Luke, B. T.; Pople, J. A.; Schleyer, P. v. R.; Clark, T., Theoretical study of the carbenoid CH₂FLi: structures and energies of the stable configurations and transition states. *Chem. Phys. Lett.* **1983**, *102* (2-3), 148-54.
72. Qiu, H.; Deng, C., Ab initio studies on the structures and isomerization of the carbenoids CH₂LiX (X = F, Cl). *Chem. Phys. Lett.* **1996**, *249* (3,4), 279-83.
73. Hermann, H.; Lohrenz, J. C. W.; Kuhn, A.; Boche, G., The influence of the leaving group X (X = F, Cl, Br, I, OH) on the carbenoid nature of the carbenoids LiCH₂X and XZnCH₂X- a theoretical study. *Tetrahedron* **2000**, *56* (25), 4109-15.

74. Boche, G.; Lohrenz, J. C. W., The Electrophilic Nature of Carbenoids, Nitrenoids, and Oxenoids. *Chem. Rev.* **2001**, *101* (3), 697-756.
75. Pratt, L. M.; Ramachandran, B.; Xidos, J. D.; Cramer, C. J.; Truhlar, D. G., Structures and Aggregation States of Fluoromethylithium and Chloromethylithium Carbenoids in the Gas Phase and in Ethereal Solvent. *J. Org. Chem.* **2002**, *67* (22), 7607-12.
76. Pratt, L. M.; Le, L. T.; Truong, T. N., A Computational Study of Mixed Aggregates of Chloromethylithium with Lithium Dialkylamides. *J. Org. Chem.* **2005**, *70* (21), 8298-302.
77. Pratt, L. M.; Phan, D. H. T.; Tran, P. T. T.; Van Nguyen, N., Basis set and electron correlation effects on lithium carbenoid dimerization energies. *Bull. Chem. Soc. Jpn.* **2007**, *80* (8), 1587-96.
78. Wang, B.; Deng, C.; Xu, L.; Tao, F., Novel structure and ring-opening mechanism of cyclopropylidene lithium fluorocarbenoid. *Chem. Phys. Lett.* **1989**, *161* (45), 388-92.
79. Sigal, N.; Apeloig, Y., Are disilacyclopropylidenes and their carbenoids good precursors for the unknown 1,3-disilaallenes? *J. Organomet. Chem.* **2001**, *636* (1-2), 148-56.
80. Azizoglu, A.; Balci, M.; Mieusset, J.-L.; Brinker, U. H., Substituent Effects on the Ring-Opening Mechanism of Lithium Bromocyclopropylidenoids to Allenes. *J. Org. Chem.* **2008**, *73* (21), 8182-8.
81. Valtazanos, P.; Elbert, S. T.; Ruedenberg, K., Ring opening of cyclopropylidenes to allenes: reactions with bifurcating transition regions, free internal motions, steric hindrances, and long-range dipolar interactions. *J. Am. Chem. Soc.* **1986**, *108* (11), 3147-9.
82. Valtazanos, P.; Elbert, S. T.; Xantheas, S.; Ruedenberg, K., The ring opening of cyclopropylidene to allene: global features of the reaction surface. *Theor. Chim. Acta* **1991**, *78* (5-6), 287-326.
83. Valtazanos, P.; Ruedenberg, K., Bifurcations and transition states. *Theor. Chim. Acta* **1986**, *69* (4), 281-307.
84. Valtazanos, P.; Ruedenberg, K., The ring opening of substituted cyclopropylidenes to substituted allenes: the effects of steric and long-range electrostatic interactions. *Theor. Chim. Acta* **1991**, *78* (5-6), 397-416.
85. Basilevskii, M. V., Natural coordinates for polyatomic reactions. *Chem. Phys.* **1977**, *24* (1), 81-9.

86. Basilevskii, M. V., The topography of potential energy surfaces. *Chem. Phys.* **1982**, *67* (3), 337-46.
87. Basilevskii, M. V., The structural stability principle and branching points on multidimensional potential energy surfaces. *Theor. Chim. Acta* **1987**, *72* (1), 63-7.
88. Palmeiro, R.; Castano, O., New valley ridge inflection point associated to the bifurcation of a valley on potential energy surfaces. *Int. J. Quantum Chem.* **2007**, *107* (14), 2687-96.
89. Palmeiro, R.; Frutos, L. M.; Castano, O., Note on the theory of bifurcation of chemical reactions. *Int. J. Quantum Chem.* **2002**, *86* (5), 422-5.
90. Quapp, W., How does a reaction path branching take place? A classification of bifurcation events. *J. Mol. Struct.* **2004**, *695-696*, 95-101.
91. Quapp, W.; Hirsch, M.; Heidrich, D., Bifurcation of reaction pathways. The set of valley ridge inflection points of a simple three-dimensional potential energy surface. *Theor. Chem. Acc.* **1998**, *100* (5-6), 285-99.
92. Quapp, W.; Hirsch, M.; Heidrich, D., An approach to reaction path branching using valley-ridge inflection points of potential-energy surfaces. *Theor. Chem. Acc.* **2004**, *112* (1), 40-51.
93. Yanai, T.; Taketsugu, T.; Hirao, K., Theoretical study of bifurcating reaction paths. *J. Chem. Phys.* **1997**, *107* (4), 1137-46.
94. Seebach, D.; Siegel, H.; Muellen, K.; Hiltbrunner, K., Direct carbon-13 NMR spectroscopic observation of cyclopropylidene-bromolithium carbenoids. *Angew. Chem.* **1979**, *91* (10), 844-5.
95. Han, C.; Rangarajan, S.; Voukides, A. C.; Beeler, A. B.; Johnson, R.; Porco, J. A., Reaction discovery employing macrocycles: transannular cyclizations of macrocyclic bis-lactams. *Org. Lett.* **2009**, *11* (2), 413-6.
96. Dolata, D. P.; Spina, D. R.; Mash, E. A., Systematic search of transition state conformations. *Tetrahedron Lett.* **1992**, *33* (44), 6571-4.
97. Dolata, D. P.; Spina, D. R.; Stahl, M. T., Conformational Searching and Modeling of Transition States. *J. Chem. Inf. Comput. Sci.* **1996**, *36* (2), 228-30.
98. Wolfe, S.; Buckley, A. V.; Weinberg, N., A comprehensive computational examination of transannular Diels-Alder reactions of unsubstituted C14 trienes - Barriers, template effects, and the Curtin-Hammett principle. *Can. J. Chem.* **2001**, *79* (8), 1284-92.

99. Baldwin John, E.; Raghavan Anuradha, S.; Hess, B. A., Jr.; Smentek, L., Thermal [1,5] hydrogen sigmatropic shifts in cis,cis-1,3-cyclononadienes probed by gas-phase kinetic studies and density functional theory calculations. *J. Am. Chem. Soc.* **2006**, *128* (46), 14854-62.
100. Koslover Elena, F.; Wales David, J., Comparison of double-ended transition state search methods. *J. Chem. Phys.* **2007**, *127* (13), 134102.
101. Brown, R. F. C.; Eastwood, F. W.; Harrington, K. J.; McMullen, G. L., Methyleneketenes and methylenecarbenes. III. Pyrolytic synthesis of arylacetylenes and their thermal rearrangements involving arylmethylenecarbenes. *Aust. J. Chem.* **1974**, *27* (11), 2393-402.
102. Brown, R. F. C., Thermal rearrangements of alkynes under flash vacuum pyrolysis conditions. The acetylene-methylenecarbene rearrangement. *Recueil des Travaux Chimiques des Pays-Bas* **1988**, *107* (12), 655-61.
103. Ajaz, A., Unpublished Work, University of New Hampshire.
104. Gaussian 03, Revision E.01, Frisch, M. J.; Trucks, G. W.; Schlegel, H. B.; Scuseria, G. E.; Robb, M. A.; Cheeseman, J. R.; Montgomery, Jr., J. A.; Vreven, T.; Kudin, K. N.; Burant, J. C.; Millam, J. M.; Iyengar, S. S.; Tomasi, J.; Barone, V.; Mennucci, B.; Cossi, M.; Scalmani, G.; Rega, N.; Petersson, G. A.; Nakatsuji, H.; Hada, M.; Ehara, M.; Toyota, K.; Fukuda, R.; Hasegawa, J.; Ishida, M.; Nakajima, T.; Honda, Y.; Kitao, O.; Nakai, H.; Klene, M.; Li, X.; Knox, J. E.; Hratchian, H. P.; Cross, J. B.; Bakken, V.; Adamo, C.; Jaramillo, J.; Gomperts, R.; Stratmann, R. E.; Yazyev, O.; Austin, A. J.; Cammi, R.; Pomelli, C.; Ochterski, J. W.; Ayala, P. Y.; Morokuma, K.; Voth, G. A.; Salvador, P.; Dannenberg, J. J.; Zakrzewski, V. G.; Dapprich, S.; Daniels, A. D.; Strain, M. C.; Farkas, O.; Malick, D. K.; Rabuck, A. D.; Raghavachari, K.; Foresman, J. B.; Ortiz, J. V.; Cui, Q.; Baboul, A. G.; Clifford, S.; Cioslowski, J.; Stefanov, B. B.; Liu, G.; Liashenko, A.; Piskorz, P.; Komaromi, I.; Martin, R. L.; Fox, D. J.; Keith, T.; Al-Laham, M. A.; Peng, C. Y.; Nanayakkara, A.; Challacombe, M.; Gill, P. M. W.; Johnson, B.; Chen, W.; Wong, M. W.; Gonzalez, C.; and Pople, J. A.; Gaussian, Inc., Wallingford CT, 2004.
105. Spartan 06, Version 1.12; Wavefunction, Inc.: Irvine, CA, 2007.
106. Spartan 08, Version 1.0.0; Wavefunction, Inc.: Irvine, CA, 2008.
107. Zhao, Y.; Truhlar, D. G. *Acc. Chem. Res.* **2008**, *41*, 157.
108. (a) Becke, A. D. *J. Chem. Phys.* **1993**, *98*, 5648. (b) Lee, C.; Yang, W.; Parr, R. G. *Phys. Rev. B* **1988**, *37*, 785. (c) Stephens, P. J.; Devlin, F. J.; Chabalowski, C. F.; Frisch, M. J. *J. Phys. Chem.* **1994**, *98*, 11623-11627. (d) Riley, K. E.; Op't Holt, B. T.; Merz, K. M., Jr. *J. Chem. Theory Comput.* **2007**, *3*, 407. (e) Tirado-Rives, J.; Jorgensen, W. L. *J. Chem. Theory and Comput.*; **2008**; *4*, 297-306.

109. (a) Tomasi, J.; Persico, M. *Chem. Rev.* **1994**, *94*, 2027. (b) Amovilli, C.; Barone, V.; Cammi, R.; Cancès, E.; Cossi, M.; Mennucci, B.; Pomelli, C. S.; Tomasi, J. *Adv. Quant. Chem.* **1998**, *32*, 227.

110. (a) Halgren, T.A. *J. Comput. Chem.* **1996**, *17(5&6)*, 490-519. (b) Halgren, T.A.; Nachbar, R.B. *J. Comput. Chem.* **1996**, *17(5&6)*, 587-615.

APPENDIX

APPENDIX A: COMPUTATIONAL DETAILS

General Methodology

Calculations were carried out with Gaussian 03¹⁰⁴, Spartan 06¹⁰⁵, or Spartan 08¹⁰⁶. Geometry optimizations used either the M05-2X¹⁰⁷ or B3LYP¹⁰⁸ functional, followed in some instances by a single point CCSD(T) calculation. Unscaled DFT zero-point corrections were applied to all energies. Structures were characterized as minima or first order saddle points by vibrational frequency analysis. Where appropriate, intrinsic reaction coordinate calculations confirmed the proper transition state linking reactants and products. Implicit solvation models used the Polarizable Continuum Model.¹¹⁰

Chapter I

For some open-shell diradicals, notably **5**, single point CCSD(T) calculations were successful only when using the quadratically convergent SCF program with very tight linear convergence. Open shell singlets were computed with a broken symmetry guess (guess=mix).

Chapter II

For many of the bicyclic carbenoids, optimizations and IRC calculations in cartesian coordinates were successful when those in internal coordinates were not.

Chapter IV

The [1,2] H-shift transition states were located by starting with the vinylidene structure and manually lengthening the C-H bond of the migrating hydrogen and decreasing the H-C=C angle to ~78 degrees.